Accepted Manuscript

Design, synthesis and biological evaluation of 2-hydrazinyladenosine derivatives as A_{2A} adenosine receptor ligands

Min Zhang, Shiyong Fan, Xinbo Zhou, Fei Xie, Song Li, Wu Zhong

PII: S0223-5234(19)30577-X

DOI: https://doi.org/10.1016/j.ejmech.2019.06.050

Reference: EJMECH 11453

To appear in: *European Journal of Medicinal Chemistry*

Received Date: 4 April 2019

Revised Date: 10 June 2019

Accepted Date: 17 June 2019

Please cite this article as: M. Zhang, S. Fan, X. Zhou, F. Xie, S. Li, W. Zhong, Design, synthesis and biological evaluation of 2-hydrazinyladenosine derivatives as A_{2A} adenosine receptor ligands, *European Journal of Medicinal Chemistry* (2019), doi: https://doi.org/10.1016/j.ejmech.2019.06.050.

Design, synthesis and biological evaluation of 2-hydrazinyladenosine derivatives as A_{2A} adenosine receptor ligands

Min Zhang[a,b], *Shiyong Fan*[a], *Xinbo Zhou*[a], *Fei Xie*[a], *Song Li*[a,*], *Wu Zhong*[a,*]

[a] National Engineering Research Center for the Emergency Drug, Beijing Institute of Pharmacology and Toxicology, Beijing 100850, PR China

[b] General Hospital of Tibet Military Command, Lhasa, Tibet, 850007, PR China

[*] Corresponding author

Wu Zhong: National Engineering Research Center for the Emergency Drug, Beijing Institute of Pharmacology and Toxicology, China; E-mail: zhongwu@bmi.ac.cn

Song Li: National Engineering Research Center for the Emergency Drug, Beijing Institute of Pharmacology and Toxicology, China; E-mail: lis.lisong@gmail.com

We discovered a novel agonist for the A_{2A}AR for the first time, and optimized the structure of a known agonist, Regadenoson, to potent higher activity agonist for the A_{2A}AR.

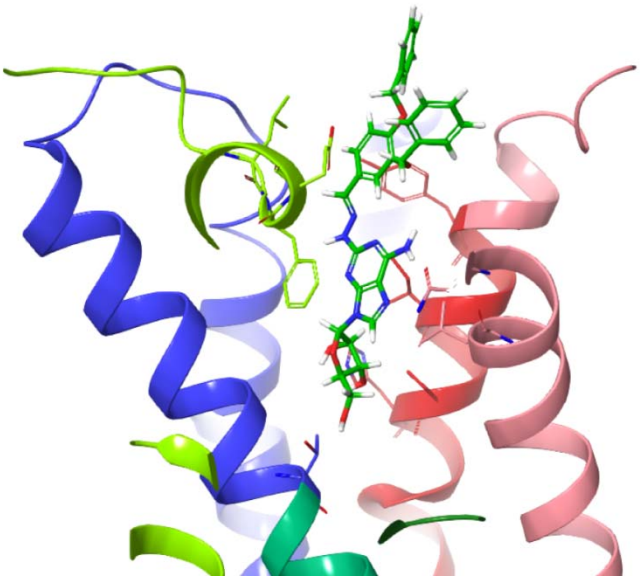

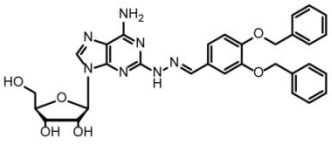

23

hA_{2A} binding K_i = 1.8 nM
hA_{2A} functional EC_{50} = 0.64 nM
Binding selectivity, A_1/A_{2A} > 1000 fold

Design, synthesis and biological evaluation of 2-hydrazinyladenosine derivatives as A_{2A} adenosine receptor ligands

Min Zhang[a,b], *Shiyong Fan*[a], *Xinbo Zhou*[a], *Fei Xie*[a], *Song Li*[a,*], *Wu Zhong*[a,*]

[a] National Engineering Research Center for the Emergency Drug, Beijing Institute of Pharmacology and Toxicology, Beijing 100850, PR China

[b] General Hospital of Tibet Military Command, Lhasa, Tibet, 850007, PR China

[*] Corresponding author

Wu Zhong: National Engineering Research Center for the Emergency Drug, Beijing Institute of Pharmacology and Toxicology, China; E-mail: zhongwu@bmi.ac.cn

Song Li: National Engineering Research Center for the Emergency Drug, Beijing Institute of Pharmacology and Toxicology, China; E-mail: lis.lisong@gmail.com

ABSTRACT

To obtain potential A_{2A} adenosine receptor agonists, a series of 2-hydrazinyladenosine derivatives were synthesized and assayed for adenosine receptors activity using radioligand binding activity assays. The binding activity of the subtypes was examined, and the structure-activity relationship of this class of compounds at the A_{2A} receptor was investigated. A fragment-based computer-aided design method was used to modify the 2-position side chain structures with different structural fragments, and the newly generated molecules were docked to the A_{2A} receptor to assess scoring and screening activity. To synthesize compounds with better scoring activity, the newly synthesized compounds were tested for in vitro receptor binding activity. 2-Hydrazinyladenosine derivatives of 32 new structural types were designed and synthesized, with the most potent adenosine derivative 23 exhibiting a K_i value of 1.8 nM for A_{2A}AR and significant selectivity for the A_{2A} receptor compared to the A_1 receptor. In addition to, compound 23, 24, 30, 31, and 42 also exhibited potent A_{2A} receptor selectivity, with Ki values for the A_{2A} receptor of 6.4, 20, 67 and 6.3 nM, respectively. We also found that compound 35 has a high A_1 receptor selectivity, with a K_i value for the A_1 receptor of 4.5 nM. Further functional assays also demonstrated that these compounds have potent A_{2A} receptor

agonist activity. The study shows the applicability of an in silico fragment-based molecular design for rational lead optimization in A_{2A}AR.

Keywords: G Protein-Coupled Receptors; A_{2A} Agonist; Fragment-Based Drug Design.

1. Introduction

Adenosine (1, **Figure 1**) is a well-known intermediate of purine synthesis and energy metabolism, and is one of the human body's most important neuromodulators that interacts with four pharmacologically classified G protein-coupled receptors (GPCRs), including the A_1, A_{2A}, A_{2B} and A_3 adenosine receptors (ARs) [1, 2]. The key role of the A_{2A}AR in various pathophysiological conditions, especially immunosuppressive disorders, inflammatory tissue damage, and neurodegenerative diseases such as Parkinson's disease (PD), Huntington's disease, and Alzheimer's disease, has been extensively investigated [3-6]. Since the A_{2A}AR is widely distributed in the human body, agonists and antagonists of the A_{2A}AR are recommended for the treatment of various pathological conditions. Adenosine (**1**, hA_{2A} K_i = 700 nM) [7] mediates the A_{2A}AR to produce potent immunosuppressive and hypotensive effects. Some of the major potential therapeutic effects of A_{2A}AR agonists are anti-inflammatory and immunosuppressive effects, which occur through modulation of the activity of neutrophils, macrophages, and T lymphocytes. In the cellular signaling pathway, A_{2A}AR activation suppresses the NF-kB pathway, diminishes inflammatory cytokines, such as tumor necrosis factor α (TNF-α), interleukin-1 β (IL-1 β), IL-8, and IL-6, and inhibits metalloproteinase 1 (MMP-1) and MMP-3 release. Therefore, selective agonists have been developed to potentially treat related conditions such as allergic rhinitis, asthma, and chronic obstructive pulmonary disease [3, 8]. However, the systemic use of A_{2A}AR agonists as anti-inflammatory drugs is limited, due to stimulation of the heart and blood vessels and potent hypotensive activity, as activation of the A_{2A}AR produces an anti-inflammatory effect [9]. On the other hand, A_{2A}AR agonists are potent vasodilators that are applied as diagnostic agents for pharmacologic stress testing of the heart. Although A_{2A}AR agonists as potent vasodilators have been associated with systemic side effects, low doses reportedly may not produce significant cardiovascular side effects. In addition, further potential therapeutic applications for A_{2A}AR agonists include treatment of psychosis and Huntington's disease [10, 11]. A_{2A}AR agonists have been shown to have neuroprotective effects in

neurodegenerative disorder models by reducing excitatory neurotransmitter release, apoptosis and inflammatory responses [5, 12].

Figure 1.

Currently, the crystal structures of A_{2A}AR in complex with its ligand or inhibitor have been delineated in several successive studies in the last few years [13-21], and the situation is rapidly changing with breakthroughs in AR crystallography since the X-ray crystal structures discussed here represent the best tools to inspire rational ligand design. The crystal structures of the A_{2A}AR complex show the patterns of binding to different small molecules and changes in the structural conformations of the A_{2A}AR including the inactive state, the intermediate state and the active state. The conformationally selective A_{2A}AR agonist, 2-(3-(1-(pyridin-2-yl)piperidin-4-yl) ureido)ethyl-6-N-(2,2-diphenylethyl)-5'-N-ethyl-carboxamido- adenosine-2-carboxamide (UK-432097, **5, Figure 1**)[21] is capable of receptor stabilization in a specific active state configuration (PDB ID: 3QAK), while the conformationally selective A_{2A}AR antagonist 4-(2-[7-amino-2-(2-furyl)- [1,2,4]triazolo[2,3-α]- [1,3,5]triazin-5-ylamino]ethyl)phenol (ZM241385) [14-16, 19] can stabilize the inactive state of the receptor (PDB ID: 3EML, 3PWH, 3VGA, 4EIY). In addition, in the X-ray structures of the A_{2A}AR bound to its endogenous agonist adenosine (**1**)[18], the synthetic analogue 5'-(N-ethylcarboxamido)adenosine (NECA, **2, Figure 1**, hA_{2A} K_i = 20 nM) [18], and the agonist CGS21680(**4, Figure 1**)[17], the A_{2A}AR retains an intermediate state conformation. The crystal structure complex has recently been determined, revealing that agonists induce motion of helices 3, 5 and 7 while antagonists prevent conformational change of the receptor [21]. The crucial residues of the A_{2A}AR within the seven TM domains interacting with the ligand are oriented toward the extracellular portion of the receptor and are highly conserved [16]. In addition, the hydrophilic binding pocket occupied by the ribose residue of agonists is different from the position occupied by antagonists.

Although a few nonselective A_{2A} ligands have been used as tools to understand the pharmacology of A_{2A} receptors, we focused on A_{2A} selective agonists, such as CGS21680 (**4**), to reduce the complexity of associated pharmacological effects. Similar to CGS21680 (**4**, hA_{2A} K_i = 27 nM[22, 23], hA_1AR K_i = 290 nM[24]), the main feature of other known selective A_{2A}AR agonists is the presence of bulky substituents at the 2-position of the adenine bicycle. In our

current research, we focused on 2-[N-1-(4-N-methylcarboxamidopyrazolyl)]-adenosine (Regadenoson, Lexiscan^{TM}, **3, Figure 1**) [25]. Regadenoson (**3**), an A_{2A}AR agonist, was approved in 2008 by the Food and Drug administration (FDA) for stress testing in conjunction with myocardial perfusion imaging because of its vasodilatory effects via activation of the A_{2A}AR [26, 27]. For the design of new A_{2A}AR agonists, we analyzed the crystal structure complex, which provided fundamental information regarding the receptor-ligand interaction based on the crystal structures of known A_{2A}AR agonists. Then, we resynthesized and evaluated regadenoson (**3**) and optimized 2-hydrazinoadenosine of the synthetic intermediate of regadenoson (**3**) as a starting template for modifications. Once the template was determined, we started a research program to design a series of new compounds that could serve as potent and selective A_{2A}AR agonists for BBBD through a structure-based drug design (SBDD) approach to comprehensively explore and replace the 4-N-methylcarboxamidopyrazolyl moiety of regadenoson (**3**) with different alkyl or aralkyl moieties. Finally, the designed compounds were synthesized, and the effects of the new modifications of the A_{2A}AR as well as the A_1AR were evaluated and are reported in the present study.

2. Results and Discussion

2.1 Fragment-Based Structure Design.

The direct design and synthesis of a large number of structural derivatives to discover new active compounds represent a very economical and time-consuming task. Structural optimization and prediction through computational methods are the best options for reducing experiment costs and saving time. Fragment-based drug design methods use one or more fragment libraries to construct ligands, and the generated small molecules are very likely to have strong interactions with biological targets. The success of these methods depends on two main aspects: the effectiveness of the design strategy and the generation of fragments with a rational structure design. As fragment databases play an important role in the drug design of a fragment, we prefer the construction of a set of molecular fragment libraries. For molecular fragment libraries, the separation rules of compound molecules are very important for the quality of the generated fragment library and application purposes. For example, RECAP[28] is a classical method of splitting molecular fragments, which include 11 splitting rules based on inverse synthetic chemistry that facilitate the synthesis and design of structural molecules. When designing new

molecules, we can select the appropriate flexible segment structure to construct the derivative group; thus, we need the split-segment rule to distinguish between rigid and flexible structures. Therefore, we use the ring and chain splitting rule[29]. According to the predefined splitting rules[29], we extracted 337,441 compound molecules from the MDDR database and decomposed all the compounds to 741706 rigid ring segments, 6666155 flexible side chains and 358023 flexible link chain structures while removing duplicates of the same structure. The fragment, which is a uniquely structured, has a total of 31197 structures (9404 rigid ring segments, 11222 side chains, and 10571 linkage strands) for construction of the fragment library. Energy optimization and structural assessment of each fragment is performed while building the fragment library. Extraction of molecular fragments from known drug molecules or candidate drug molecules using the MDDR database can reduce the possibility of toxic fragment structures and increase the probability of successful drug design.

High economic and time costs are barriers to the synthesis of a large quantity of structural derivatives. Computational approaches are the best alternative to experimental methods. We developed molecule design strategies using CombLig, to design derivative compounds based on the three-dimensional structure of the active sites of target enzymes. An overview of our strategy in CombLig is schematically illustrated in **Figure 2**. The CombLig program provides two strategies to build derivative molecules and requires fragment libraries to generate ligand structures (see the Experimental Section). We hope to create some high-quality structural derivatives that include the structural information of a known drug, including the molecular stability, toxicity, bioavailability, synthetic feasibility, and other related information.

Figure 2.

In further design research, we used the crystal structure of the A_{2A}AR complex from the Protein Data Bank (entry 3QAK). In this complex structure, agonist molecule UK432097 (**5**) is present (see **Figure 3a**), which appropriately fits the binding pocket, occupies most of the A_{2A}AR ligand-binding site, and shows high binding affinity and subtype selectivity. The binding site reveals a well-characterized protein-ligand interaction map in this case, including 11 hydrogen bonds, one aromatic stacking integration, and several nonpolar (van der Waals) interactions[21]. However, UK432097 (778 daltons) is too large to serve as a seed substructure to

design new molecules because it occupied almost all regions in the active site. We found that UK432097 (**5**) and Regadenoson (**3**) have a common scaffold of the bicyclic adenine core, which is present in almost all A_{2A}AR agonists. Regadenoson (**3**) is an FDA-approved A_{2A}AR agonist for cardiac contrast auxiliaries, and its adenine ring 2-position side structure is much smaller than that of UK432097 (**5**); thus the space for structural design is relatively larger. Therefore, the compound Regadenoson (**3**) was docked into the binding pocket of the A_{2A}AR by DOCK6 to determine the complex conformation of Regadenoson (**3**) and the A_{2A}AR (See **Figure 3a**). The docking structure study showed that the 2-position synthetic intermediate of Regadenoson (**3**), 2-hydrazinoadenosine (**11**), could be used as a good design starting structure because the ideal lead compound should consist of smaller structures and remain at the receptor binding sites with a reasonable position and orientation. Additionally, from a synthetic point of view, the hydrazino structure is easy to connect with new structures.

Therefore, we used CombLig strategies A and B described above to construct new 2-hydrazinoadenosine derivatives starting from the 2' amino group of 2-hydrazinoadenosine, and the designed compounds were further docked, scored and screened. In strategy A, the fragment is grown on the 2' amino group of 2-mercaptoadenosine that has been docked to the A_{2A}AR active site, and the characteristics of the active site act as constraints to filter the new molecules to retain molecules that interact with key areas of the active pocket. At this time, the newly generated molecules are not subjected to energy minimization, and the conformations of the new molecules maintain a pattern of speculated binding with the receptor. The resulting new molecules achieved their energy-optimized conformation through an energy minimization process, and the root-mean-square deviation (rmsd) values between the energy-optimized conformations of the new molecules and the conformations of estimated combined modes were calculated. The purpose of calculating the rmsd values is to examine the deviation between the speculated-bound conformation and the energy-optimized conformation to determine whether the conformation of the fragment maintains the original binding pattern in the final molecule, which indicates whether the linking fragment significantly alters its binding to the receptor in the final combined mode of the compound. Therefore, the rmsd values reflecting the differences between the energy-optimized conformations and the combined conformations are used as scoring functions to evaluate the new molecules, and the molecules with less deviation from the conformation of the original constituent fragments in the active site are ultimately selected.

Compounds with rmsd values below a certain threshold are considered high-potency active ligands, and this rmsd-based scoring function facilitates compound selection in new compound libraries. The advantage of using this strategy is that the best fragments that interact with residues in the active site can be found based on the characteristics of the receptor site.

Design strategy B in CombLig mainly aims to improve the structural diversity of the newly generated molecules. We directly connected the fragment with the starting structure, the 2' amino group of 2-hydrazinoadenosine, the newly generated molecules were docked to the A_{2A}AR active site, and the scoring function was used for evaluation and entered to the design program to continue the next construction procedure. The energy minimization process is not performed with this strategy to enable the constituent fragments of the final compounds to retain their docking binding conformations at the active site. The scoring function implemented in the molecular docking program is used to sort new molecules. Compared to strategy A, strategy B can better reflect changes in the overall binding mode of the new molecule at the active site of the receptor. This strategy may yield more combinations of fragments. However, the disadvantage of strategy B is that the process of generating new molecules is not subject to receptor constraints, and the number of new molecules produced can be considerably larger than the number produced using strategy A. We used a variety of methods to limit and filter new molecules according to basic properties and key pharmacodynamics, for example, Lipinskis' rule, ADMET (absorption, distribution, metabolism, elimination, toxicity) limits or other standard methods which can reduce molecule production. Through these two strategies, according to the receptor binding mode and synthetic treatability of the new molecules, we finally designed and selected 32 new molecules (**12-43**) as synthetic research objects and verified their biological activity as potent A_{2A}AR agonists.

2.2 Chemistry.

The general synthetic approach used to prepare the new N'-substituted-2-hydrazinyladenosines **12-43** is depicted in **Scheme 1**. As shown, the compound 2,6-dichloropurine (**7**) was coupled with ribofuranose tetraacetate (**6**) to produce the triacetate nucleoside compound of 2,6-dichloro-9-(2',3',5'-tri-*O*-acetyl-β-D-ribofuranosyl)purine (**8**). The acetate groups of 2,6-dichloro-9-(2',3',5'-tri-*O*-acetyl-β-D-ribofuranosyl)purine (**8**) were subsequently hydrolyzed, and the resultant 2,6-dichloro-9-(β-D-ribofuranosyl)purine(**9**) was

reacted with saturated ammonia in ethanol solution to produce the 2-chloroadenosine nucleoside (**10**). The 2-chloro group of 2-chloroadenosine (**10**) can then be converted to a hydrazine derivative of 2-hydrazinoadenosine(**11**) through a hydrazinolysis reaction. Treating the 2-hydrazinoadenosine (**11**) in methanol with aralkyl aldehyde or alkyl aldehyde for half an hour generated the corresponding 2-hydrazinyladenosines **12-43**.

Scheme 1.

The 2-hydrazinyladenosines were precipitated from methanol except for **14-16, 18, 20, 33-34, and 40-43**, which were further purified using silica gel column chromatography. The 2-hydrazinyladenosines **12-43** were further purified by medium pressure liquid chromatography (MPLC) on reverse phase C18 material to remove traces of the unreacted sugars. The structures of the synthesized nucleosides were confirmed by ^{1}H and ^{13}C NMR spectroscopy and MS. All the corresponding data can be found in the Experimental Section.

2.3 Pharmacology.

The biological activity of the synthesized 2-hydrazinyladenosine **12-43** toward hA_1 and hA_{2A} receptors were investigated in vitro. Competitive binding experiments were performed using membrane preparations of the human recombinant A_1AR and $A_{2A}AR$ expressed in Chinese hamster ovarian (CHO) cells using [3H]DPCPX (cyclopentyl-1,3-dipropylxanthine) and [3H]CGS21680 as radioligands, respectively. The most potent compounds, **12, 21, 23-24, 30, 32, 34, 36, 39** and **41-43,** were also evaluated in functional assays by measuring their ability to modulate cyclic AMP levels in human embryonic kidney (HEK) 293 cells stably overexpressing human adenosine receptors, $hA_{2A}ARs$. The test results and structures of the synthesized compounds are depicted in **Table 1**.

Table 1.

2.3.1 Adenosine receptor affinity.

As mentioned above, we synthesized 32 new compounds; then, we evaluated their affinity for different compounds to identify small molecules with high affinities. In general, the measured K_i

values in the present series of newly synthesized compounds confirm the previous design strategy and the prediction results indicating that the affinity of 2-substituted adenosine derivatives depends on the attributes of the substituents in accordance with the structure-activity relationship. In the present study, 2-hydrazinyl nucleosides were synthesized and evaluated in radioligand binding studies of two AR subtypes. The K_i values obtained by binding the compounds to the receptor showed that the compounds exhibited higher affinity for the A_{2A}AR. The introduction of different side chains to the 2-position of adenosine through a hydrazone linker to form the 2-hydrazinyladenosine structure with different fragment lengths and distinct functional groups generally led to compounds with a relatively higher affinity for the A_{2A}AR rather than the A_1AR, as shown in **Table 1**.

First, we introduced a series of the substituted phenyl substructures as R groups to form compounds **12-31**. The results of affinity evaluation showed that different substituted phenyl moieties seem to produce markedly different affinities for the A_{2A}AR, with K_i values ranging from 1.8 nm to 6625 nm. The rank order of potency of compounds **12-31** at the A_{2A}AR is as follows: **23** (1.8 nm) > **21** (5.5 nm) > **24** (6.4 nm) > **12** (8.5 nm) > **30** (20 nm) > **14** (61 nm) > **31** (67 nm) > **22** (101 nm) > **20** (173 nm) > **28** (208 nm) > **29** (204 nm) > **18** (18 nm) > **26** (800 nm) > **15** (801 nm) > **13** (1306 nm) > **27** (1329 nm) > **19** (1622 nm) > **17** (5495 nm) > **16** (6276 nm) > **25** (6625 nm). Among compounds **12-31**, 2-((benzylidene)hydrazinyl)adenosine derivatives **23, 21, 24, 12, 30, 14,** and **31** showed very high affinity at the A_{2A}AR. The quantified K_i values (1.8nm - 67 nm) were generally high at the A_{2A}AR, except for compounds **12** and **14**, which showed higher affinity for the A_1AR with K_i values of 4.1 and 37 nM, respectively. For the A_1AR, compounds **23, 24,** and **31** showed very low affinity (0% inhibition), and the rank order of potency for the A_1AR was **12** (4.1 nM) > **14** (37 nM) > **21** (70 nM) > **30** (7856 nM). Compounds **15, 18, 20, 22, 26, 28,** and **29** showed moderate affinity at the A_{2A}AR with K_i values ranging from 101 to 801 nM. Among them, compounds **15, 18,** and **29** showed very low affinity at the A_1AR, and moderate affinity for the A_{2A}AR with K_i values of 801, 224 and 210 nM, respectively. However, compounds **20** and **26** showed high affinity at the A_1AR with K_i values of 13 and 2.5 nM, respectively. In addition, compounds **13, 16, 17, 19, 25,** and **27** showed low affinity at the A_{2A}AR with K_i values ranging from 1306 to 6625 nM, except for compounds **13** and **25,** which possessed high affinity at the A_1AR with K_i values of 2.9 and 5.1 nM, respectively.

To further explore the effect of the structural diversity of R substitution on affinity, we introduced aromatic heterocyclic structures as the R group. The affinity test results of compounds **32-39** for A_{2A}AR affinity ranged from 6.5 nM to 1449 nM, and these compounds also showed similar activity to that of the compounds with the substituted phenyl substructures. The rank order of potency at the A_{2A}AR was **39** (6.5 nM) > **32** (8.3 nM) > **36** (8.7 nM) > **34** (18 nM) > **33** (71 nM) > **37** (239 nM) > **38** (1449 nM). Only compound **35** had very low activity at the A_{2A}AR, which may be related to the large substituent of phenyl substructures on the furan ring. Additionally, compounds **32-39** also showed high affinity for the A_1AR. Compound **35** showed a stronger selective affinity (4.5 nm) for the A_1AR versus the A_{2A}AR. Furthermore, we also synthesized and evaluated compounds **40-43** with other types of R substituents to more fully explore the impact of R substitution on activity. Compound **40** showed unexpectedly very low affinity for both the A_1AR and A_{2A}AR, compounds **41, 42** and **43** all showed strong affinity for the A_{2A}AR, and compounds **41** and **43** also showed strong affinity for the A_1AR. In general, most of the new 2-hydrazinyl adenosine derivatives showed a specific A_{2A} affinities. The affinities of compounds **12-43** for the A_1AR were analyzed. As shown in **Table 1**, some compounds have very low affinity for the A_1AR, and some compounds have high affinity for the A_1AR including compounds **12, 13, 25, 26, 32, 35, 36, 37, 38, 39, 41,** and **43**. However, compound **35 has** only high A_1 receptor affinity. The compound with the highest affinity for the A_{2A} receptor in the present 2-hydrazinyladenosine series is compound **23**, which exhibited a K_i value of 1.8 nM and was inactive at the A_1AR subtype with a K_i value >10 μM.

2.3.2 Functional Assays of the hA_{2A}AR.

The functional properties of the most potent compounds, **12, 21, 23-24, 30, 32, 34, 36, 39** and **41-43,** were assessed by adenylate cyclase assays measuring cAMP accumulation in human HEK-293 cells stably expressing the human A_{2A}AR. Molecules showing the best affinities for hA_{2A}AR were confirmed to display high potency in the functional assay (see **Table 2**). Interestingly, concentration–response curves of the investigated compounds were obtained, which showed that the test compounds acted as complete hA_{2A}AR agonists in the cAMP functional assay. Most importantly, binding data for each ligand reflected A_{2A} agonist potency correlation with K_i and EC_{50} values in the same nanomolar range (see **Table 2**). Compound **23**,

which has the highest hA_{2A} affinity (K_i = 1.8 nM), also had the highest EC_{50} value of 0.64 nM among the series of compounds.

Table 2.

2.4 Molecular Modeling.

2.4.1 Docking the new compounds to A_{2A}AR.

Molecular modeling techniques are applied to decipher the structural basis for the effect of the binding affinity of a compound to its target protein. Molecular docking can be instrumental in analyzing the interactions of newly synthesized compounds with receptors and obtaining the binding conformations of the new compounds in the active site. Accordingly, we set out to elucidate the structural details of the binding mode of newly synthesized compounds in the A_{2A} receptor structure, such as compound **23**, which was the most promising candidate in the initial phase of designing a new A_{2A} agonist (see **Table 1**). Fourteen A_{2A}AR X-ray crystal structures were resolved. Among them, 3QAK[21] was the candidate structure used to perform docking studies of A_{2A} agonists and was considered an A_{2A} active receptor model for the docking studies. Through the docking studies, the binding modes of newly synthesized compounds within the A_{2A}AR binding site, which are depicted in **Figure 3**, were obtained.

Figure 3.

In the docked complex, the purine core of newly synthesized compounds is adapted in a similar fashion to that observed in the X-ray crystal structure of the A_{2A} receptor in complex with the agonist UK432097 (see **Figure 3a** and **3b**). Compounds that satisfied the contact criteria were deeply buried in the binding site of the receptor and typically had an adenine group which overlapped the adenine moiety of the co-crystal agonist. Similar to crystalline nucleoside agonists, the ribosyl moiety of the new compounds also occupied the ribose binding pocket. In particular, the 3'R- and 2'R-hydroxyl groups of the ribosyl moiety, which is crucial for agonist activity, formed hydrogen bonds to Ser277 and His278 in the new compounds. Most of the new compounds had interactions with Asn253 suggesting that interactions with this residue are key for ligand binding. The key interactions are (i) hydrogen bonds between the sugar moiety and the

THR88 (helix III), HIS250 (helix VI), SER277 (helix VII), and HIS278 (helix VII) residues; (ii) a hydrogen bond between the adenosine ring and ASN253 (helix VI) residue; a π-π stacked interaction between the adenosine ring and the PHE168 residue on extracellular loop 2 (ECL2); and π-Alkyl interactions between the adenosine ring and the LEU249 (helix VI) and ILE274 (helix VII) residues; (iii) a hydrophobic interaction between the 2-position side chain and the LEU167 (ECL2) residue; a π-Anion interaction between the phenyl ring on the 2-position-substituted phenylhydrazine group and the GLU169 (ECL2) residue; a π-π T-shaped interaction between the same phenyl ring and the TYR271 (helix VII) residue; and (iv) hydrophobic interactions between some 2-position long side chains and the THR256 (helix VI), LEU267 (helix VII), and MET270 (helix VII) residues (see **Figure 3c**, **3d** and **4**). On the basis of these observations, these key interactions, involving the adenine core, the ribose ring and the 2-position side chain, were noted in the docking poses of these new compounds and were considered to be the most important for the binding affinities for the A_{2A}AR.

Figure 4.

The resulting binding mode was also helpful when attempting to explain the highest activity profile of compound **23** among all newly synthesized compounds **12-43**. This observation of the binding mode is also supported by comparison of the binding mode of the agonist UK432097 (**5**) in the A_{2A}AR crystal structure reported by Xu et al. [21]. Prompted by these observations, we analyzed the conformational behavior of three phenyl rings (A, B and C) in docking modeling simulations (**Figure 3d**). Indeed, the electron-rich phenyl ring A of compound **23** is accommodated in a region lined by hydrophobic residues (LEU167 and TYR271), which in turn reinforce the π-Anion interaction with the GLU169 residue. Moreover, phenyl ring B of compound **23** was able to establish relevant interactions with the MET270 and THR256 residues, which occupied the same position as the 6-substituted phenyl ring of UK432097 (**5**) in the crystal structure. Further, phenyl ring C of compound **23** is located in the pocket entrance region of the active site where the A_{2A}AR possesses the hydrophobic residue LEU267. In this case, the three phenyl groups (A, B and C) of compound **23** are endowed with substantial flexibility. The introduction of substituents of the phenyl ring (A, B and C) connecting linkers of 2 or 3 atoms

could improve the affinity profile of compound **23** for the A_{2A}AR by increasing the interactions between the receptor and ligand, thereby stabilizing the putative bioactive conformation.

3. Conclusions

This paper reports preliminary results for our research program aiming to identify potent A_{2A}AR agonists. The method for agonist design was based on fragment-based drug design (FBDD) and fragment libraries. The fragment libraries were constructed from the MDDR library using our previously reported method[35]. These libraries include high-quality fragments for molecular design, as all of them were derived from drug molecules developed to increase applicability and reduce toxicity. We also explored the strategies of FBDD and developed a set of procedures to help up design derivatives. These strategies can employ the fragment libraries mentioned above to improve the efficiency and to increase the diversity of newly designed compounds. Using these strategies, we performed agonist design and synthesis and activity assays for the A_{2A} receptor based on the reported crystallographic complex.

The crystal structure of the active-state A_{2A}AR (PDBID:3QAK) [21] was selected as the target for the structure-based molecule design of novel 2-hydrazinyladenosine derivatives. The docking studies of known agonist Regadenoson (**3**) and comparison with ligand UK-432097 (**5**) in the crystal complex suggested overlaps of critical positions, and we successfully discovered a series of potent adenosine-based ligands with very high affinities for the A_{2A}AR. Through synthesis and biological activity testing of 32 predicted high-scoring candidates, including derivatives with substituted phenyl ring compounds, substituted aromatic heterocyclic compounds and substituted alkyl compounds, we identified twenty-three compounds with submicromolar affinities for the A_{2A}AR, including nine compounds with affinities below 10 nM. Our fragment-based molecular design strategies allowed us to identify compound **23** as one of the most potent A_{2A} agonists discovered to date (K_i hA_{2A}AR = 1.8 nM, EC_{50} hA_{2A}AR = 0.64 nM, K_i hA_1AR> 10 000 nM). These studies enabled us to uncover useful information on the structural determinants that lead to higher-affinity receptor activation. In addition, the docking studies and QSAR analysis of the newly synthesized compounds also provide insight into the structural basis for further design of novel agonists, which can potentially benefit some therapeutic applications. Overall, this study demonstrated the application of fragment-based molecular design method for the development of new agonist derivatives at the A_{2A}AR.

4. Experiment Section

4.1 Structure Design and Molecular Docking.

4.1.1 Fragment Library Construction.

The fragments in libraries were obtained using a fragment database computational method that we have described previously[29]. We extracted and selected compounds that are drug-like candidates or drugs used in clinical research from the commercial MDL Drug Data Report database (MDDR3d v2011.2). All of the extracted compounds were decomposed into fragments and duplicates were removed. Then, the fragments were energy-optimized, and hydrogen atoms were added by the Discovery Studio (v2.5) program. All of the fragments can be classified into three categories, including linkers, groups and rings and are stored in SYBYL MOL2 format.

4.1.2 Fragment-based molecule design.

CombLig, a derivative design method based on fragment-based structural design strategies, consists of several major modules, i.e. SITE-GROW, STRUCT-GROW, and GROW-ANALY (see **Figure 2**). Each module has a different purpose in CombLig, the source codes of which are written in script and C++ language. CombLig provides two strategies to produce derivative molecules: a site-growing strategy based on the receptor-ligand complex and a site-docking strategy based on the ligand.

With the site-growing strategy, the production procedure is initiated from a seed substructure in the binding site of a receptor obtained from the protein-ligand cocrystal structures or by molecular docking after superimposition onto the reference. The seed substructure originating from the ligand and the sites for growth on the seed substructure can be assigned by the user. SITE-GROW is the first module executed in the site-growing strategy, which reads the 3D structures of the pro-docked seed substructure and the target receptor and tries to replace each growth site with a given fragment. The newly formed structures will be assessed for collision with the receptor, and only the structure without collision will be selected for the new growth cycle or will be saved as the candidate molecule.

With the site-docking strategy, the basic input of STRUCT-GROW for the first step is only the seed substructure, which will serve as the initial growth structure. In the production procedure, STRUCT-GROW uses a systematic sampling algorithm to improve the efficiency of structure

generation. The generated structures will be docked into the binding site of the receptor using an external dock program, DOCK 6.7[30]. This growing process of STRUCT-GROW stops when all the structures have been docked into the receptor, and the candidate molecule can finally be constructed by repeating this procedure.

With both strategies, the constructed molecules are selected as the final candidates by GROW-ANALY. To help the user to analyze the results, GROW-ANALY first groups the resultant molecules into clusters and then assesses each newly constructed molecule to ensure its chemical feasibility and score its binding affinity for the target protein. To calculate the binding affinity score, GROW-ANALY uses an empirical procedure developed to estimate the binding free energy of a generated molecule toward the receptor protein when the 3D structure of the complex is docked. A user-defined number of molecules at the top will be selected as the final results. Each molecule will be output in a SYBYL MOL2 file. The program will also provide a log file by tabulating the file name, molecular weight, logP value, binding affinity and bioavailability score of each molecule.

4.1.3 Molecular Docking.

All docking calculations were carried out with the molecular docking tool, DOCK 6.7[30]. The compound set for docking was prepared with the DS 2.5 minimization protocols. The chiral atoms in all compounds maintains the same chiral conformation as atoms of the compounds in Section 4.2. The selected crystal structure of the A_{2A}AR for docking was a 2.7 Å crystallographic structure of the A_{2A} adenosine receptor (PDB ID: 3QAK) in complex with the agonist UK-432097 (**5**), which was retrieved from the RCSB Protein Data Bank[21]. The selected crystallized complex structure was prepared with the following protein preparation workflow. The compounds to be docked are confirmed by an enclosing box whose size is 6Å larger than the cocrystallized ligand. The enclosing box is centered on the cocrystallized ligand, which is defined as the ligand-binding site search region. In the case of the A_{2A}AR, 74 matching spheres were generated and selected by the Sphgen program, and these spheres were based on the shape of the crystallographic receptor surface. Then precalculated grids were generated by the Grid program since the grid calculation must be performed prior to docking. The Grid program also computes a bump grid to identify severe steric overlaps between the ligand atoms and the receptor atoms. The new compounds are then flexibly docked into the binding site with the

anchor-and-grow incremental construction approach in DOCK 6.7. The anchor-and-grow strategy algorithm superimposes atoms of the docked molecule onto binding site-matching spheres, which indicate putative ligand atom positions. Default settings are maintained for all remaining parameters. The energy score for each conformation is calculated based on the implementation of force field scoring. Force field scores are the sum of molecular mechanical interaction energies, which consist of the receptor-ligand electrostatic and van der Waals interaction energies. The best conformation of each docked molecule includes the output based on the best score and interactions formed between the compounds and the receptor.

4.2 Synthesis.

Reaction progress and product mixtures were monitored by thin-layer chromatography (TLC) using precoated silica gel plates (Yantai dexin Bio-Technology Co., Ltd., Yantai, China) and were visualized by a UV lamp (254 nm light source). Column chromatography was performed on 200-300-mesh silica gel (Yantai Chemistry Industry Research Institute, Yantai, China). The purity of the final products was confirmed by MPLC by dissolving 10 mg/mL of the products in DMSO. A 1 mL sample was injected into an MPLC instrument (Tianjin Bonna-Agela Technologies Co., Ltd., Tianjin, China) using the C18 column (Biotage Trading Co., Ltd, Shanghai, China). Elution was performed with a gradient of water/methanol from 90:10 to 0:100 for 40 min at a flow rate of 25 mL/min, with the gradient started after 10 min. The purity of the products was generally ≥95%. The ^{1}H-NMR or ^{13}C-NMR spectra were recorded in $CDCl_3$ or DMSO-d_6 solutions using a JNM-ECA-400 400 MHz spectrometer (JEOL Ltd., Tokyo, Japan). Chemical shifts are presented as δ values (ppm) downfield from tetramethylsilane (TMS), which serves as the internal reference, and coupling constants (J) were expressed in Hz. The MS spectra were determined on an API 3000 triple-quadrupole mass spectrometer (AB Sciex, Concord, ON, Canada) coupled with a Turbo IonSpray electrospray ionization (ESI) source for mass analysis and detection. The melting points for purified products were determined on a RY-1 apparatus (Tianda Tianfa Technology Co., Ltd., Tianjin, China).

2,6-Dichloro-9-(2',3',5'-tri-O-acetyl-β-D-ribofuranosyl)purine (**8**). First, 21 g of ribofuranose tetraacetate (**6**) was heated to 90℃ until it became clear, and 12 g of 2,6-dichloropurine (**7**) and 0.3 g of stannic chloride were added with stirring. The reaction was further heated and stirred at

120℃ for 15 min. The solvent was evaporated under a vacuum, and the residue was cooled. Methanol (50ml) was added to the residue, and the solid isolated by filtration yielded the crude product. The crude product was recrystallized from ethanol to yield 12 g of 2,6-dichloro-9-(2',3',5'-tri-O-acetyl-β-D-ribofuranosyl)purine.

2-Chloroadenosine (**10**). First, 10 g of 2,6-dichloro-9-(2',3',5'-tri-O-acetyl-β-D-ribofuranosyl)-purine (**8**) in 200 mL of methanolic ammonia solution was heated to 100℃ for 24 hours in an autoclave. The solution was further stirred for an additional 24 hours at room temperature, and then the solution was subsequently evaporated to dryness under reduced pressure to remove ammonia. The residue was purified by flash chromatography using an appropriate mixture of $CHCl_3$ and MeOH as an eluent. The product was dried at 50℃ to yield 4.5g of 2-chloroadenosine as a solid.

2-Hydrazinoadenosine (**11**). First, 5 g of 2-chloroadenosine (**10**) in 25ml of hydrazine hydrate (65% in water) was stirred while heating to 50℃ for 4 hours until 2-chloroadenosine (**11**) disappeared according to TLC (CH_2Cl_2:MeOH = 3:1). The reaction mixture was then brought to 25℃ and diluted with 2-propanol (50ml) with stirring overnight. The resulting precipitate was isolated by filtration to yield 4.4g of 2-hydrazinoadenosine as a yellow solid.

General procedure for the synthesis of compounds (**12-43**). First, 0.5 g of 2-hydrazinoadenosine (**11**) and different aralkyl or alkyl aldehyde compounds (1.1 equivalent) were combined in methanol (30ml) and heated by microwave at 80℃ for 30 min. The crude products (**12-13, 17, 19, 21-32,** and **35-39**) were precipitated from methanol, and the other products (**14-16, 18, 20, 33-34,** and **40-43)** were purified from the reaction mixture using silica gel column chromatography. All the crude products were further purified by MPLC on reverse phase C18 material to yield the products (**12-43**).

4-((E)-(2-(6-amino-9-((2R,3R,4S,5R)-3,4-dihydroxy-5-(hydroxymethyl)tetrahydrofuran-2-yl)-9H-purin-2-yl)hydrazono)methyl)benzonitrile (**12**). 54% yield as a white solid; m.p. 276℃; ^{1}H NMR (DMSO-d_6): δ (ppm) 10.99 (s, 1H), 8.11 (s, 1H), 8.07 (s, 1H), 7.91 (d, 2H, J=8.4Hz), 7.83 (d, 2H, J=8.0Hz), 7.13 (br, 2H), 5.81 (d, 1H, J=6.4Hz), 5.44 (d, 1H, J=6.4Hz), 5.28-5.26 (m, 1H), 5.15 (d, 1H, J= 4.8Hz), 4.72-4.67 (m, 1H), 4.23-4.20 (m, 1H), 3.98 (d, 1H, J=2.4Hz), 3.75-3.57 (m, 2H); ^{13}C NMR (DMSO-d_6): δ (ppm) 156.26, 155.92, 150.79, 140.24, 138.22,

137.57, 132.48, 126.74, 119.04, 115.70, 109.96, 87.77, 86.03, 73.08, 71.02, 61.93; HRMS (ESI+) m/z $[M + H]^+$ calculated for $C_{18}H_{18}N_8O_4$: 411.1524; found: 411.1525.

2-((E)-(2-(6-amino-9-((2R,3R,4S,5R)-3,4-dihydroxy-5-(hydroxymethyl)tetrahydrofuran-2-yl)-9H-purin-2-yl)hydrazono)methyl)benzonitrile (**13**). 52% yield as a white solid; m.p. 260℃; ^{1}H NMR (DMSO-d_6): δ (ppm) 11.21 (s, 1H), 8.45 (s, 1H), 8.35 (d, 1H, J=8.0Hz), 8.08 (s, 1H), 7.83 (d, 1H, J=7.6Hz), 7.72 (t, 1H, J=7.6Hz), 7.48 (t, 1H, J=7.6Hz), 7.18 (br, 2H), 5.81 (d, 1H, J=6.4), 5.47 (d, 1H, J=5.6Hz), 5.29-5.27 (m, 1H), 5.17 (d, 1H, J=3.6Hz), 4.73-4.71 (m, 1H), 4.23 (s, 1H), 3.98 (s, 1H), 3.75-3.58 (m, 2H); ^{13}C NMR (DMSO-d_6): δ (ppm) 156.28, 155.80, 150.75, 138.55, 138.32, 134.69, 133.17, 132.96, 128.54, 125.14, 117.36, 115.80, 109.41, 87.84, 86.07, 73.01, 71.08, 61.95; HRMS (ESI+) m/z $[M + H]^+$ calculated for $C_{18}H_{18}N_8O_4$: 411.1524; found: 411.1523.

(2R,3R,4S,5R)-2-(6-amino-2-(2-((E)-4-(trifluoromethyl)benzylidene)hydrazineyl)-9H-purin-9-yl)-5-(hydroxymethyl)tetrahydrofuran-3,4-diol (**14**). 53% yield as a white solid; m.p. 260℃; ^{1}H NMR (DMSO-d_6): δ (ppm) 10.97 (s, 1H), 8.14 (s, 1H), 8.08 (s, 1H), 7.96 (d, 2H, J=8.4Hz), 7.74 (d, 2H, J=8.4Hz), 7.18 (br, 2H), 5.82 (d, 1H, J=6.4Hz), 5.47 (d, 1H, J=5.6Hz), 5.29 (s, 1H), 5.18 (d, 1H, J=3.2Hz), 4.71-4.69 (m, 1H), 4.23 (s, 1H), 3.98 (d, 1H, J=2Hz), 3.76-3.60 (m, 2H); ^{13}C NMR (DMSO-d_6): δ (ppm) 156.20, 155.94, 150.85, 139.63, 138.24, 137.99, 128.23, 126.78, 125.50, 123.02, 115.61, 87.78, 86.05, 73.10, 71.06, 61.95; HRMS (ESI+) m/z $[M + H]^+$ calculated for $C_{18}H_{18}F_3N_7O_4$: 454.1445; found: 454.1446.

(2R,3R,4S,5R)-2-(6-amino-2-(2-((E)-4-chloro-3-(trifluoromethyl)benzylidene)hydrazineyl)-9H-purin-9-yl)-5-(hydroxymethyl)tetrahydrofuran-3,4-diol (**15**). 54% yield as a white solid; m.p. 242℃; ^{1}H NMR (DMSO-d_6): δ (ppm) 10.94 (s, 1H), 8.46 (s, 1H), 8.07 (s, 1H), 8.01 (s, 1H), 7.89 (d, 1H, J=8.0Hz), 7.68 (d, 1H, J=8.4Hz), 7.13 (br, 2H), 5.73 (d, 1H, J=7.2Hz), 5.46 (d, 1H, J=5.2Hz), 5.39 (d, 1H, J=6.4Hz), 5.14 (s, 1H), 4.79-4.77 (m, 1H), 4.12 (s, 1H), 3.96 (s, 1H), 3.68-3.51 (m, 2H); ^{13}C NMR (DMSO-d_6): δ (ppm) 156.32, 155.98, 150.56, 138.79, 137.23, 135.40, 131.83, 129.62, 127.00, 125.141, 124.32, 121.59, 115.97, 88.34, 86.47, 72.55, 71.31, 62.27; HRMS (ESI+) m/z $[M + H]^+$ calculated for $C_{18}H_{17}ClF_3N_7O_4$: 488.1055; found: 488.1055.

(2R,3R,4S,5R)-2-(6-amino-2-(2-((E)-2,4-bis(trifluoromethyl)benzylidene)hydrazineyl)-9H-purin-9-yl)-5-(hydroxymethyl)tetrahydrofuran-3,4-diol (**16**). 54% yield as a white solid; m.p. 239℃; ^{1}H NMR (DMSO-d_6): δ (ppm) 11.44 (s, 1H), 8.70 (d, 1H, J=8.4Hz),8.47 (s, 1H), 8.12-8.01 (m, 3H), 7.31 (br, 2H), 5.81 (d, 1H, J=6.4Hz), 5.47 (br, 1H), 5.30 (br, 1H), 5.19 (br, 1H), 4.73-4.71 (m, 1H), 4.25-4.24 (m, 1H), 4.00-3.98 (m, 1H), 3.77-3.62 (m, 2H); ^{13}C NMR (DMSO-d_6): δ (ppm) 156.11, 155.37, 150.67, 138.68, 137.73, 133.15, 129.20, 127.70, 126.04, 125.73, 124.95, 122.85, 122.22, 115.89, 87.94, 86.03, 73.06, 71.04, 61.93; HRMS (ESI+) m/z $[M + H]^+$ calculated for $C_{19}H_{17}F_6N_7O_4$: 522.1319; found: 522.1319.

(2R,3R,4S,5R)-2-(6-amino-2-(2-((E)-3,4,5-trimethoxybenzylidene)hydrazineyl)-9H-purin-9-yl)-5-(hydroxymethyl)tetrahydrofuran-3,4-diol (**17**). 44% yield as a white solid; m.p. 246℃; ^{1}H NMR (DMSO-d_6): δ (ppm) 10.68 (s, 1H), 8.01 (s, 1H), 7.98 (s, 1H), 7.16 (s, 2H), 7.09 (br, 2H), 5.75 (d, 1H, J=7.2Hz), 5.49-5.45 (m, 2H), 5.12 (s, 1H), 4.92-4.88 (m, 1H), 4.15 (s, 1H), 3.99 (s, 1H), 3.84 (s, 6H), 3.68 (s, 3H), 3.72-3.52 (m, 2H); ^{13}C NMR (DMSO-d_6): δ (ppm) 156.22, 153.06, 150.60, 140.42, 138.76, 137.94, 131.09, 115.82, 103.90, 88.59, 86.43, 72.28, 71.31, 62.54, 60.06, 55.84; HRMS (ESI+) m/z $[M + H]^+$ calculated for $C_{20}H_{25}N_7O_7$: 476.1888; found: 476.1887.

(2R,3R,4S,5R)-2-(6-amino-2-(2-((E)-4-propoxybenzylidene)hydrazineyl)-9H-purin-9-yl)-5-(hydroxymethyl)tetrahydrofuran-3,4-diol (**18**). 41% yield as a white solid; m.p. 218℃; ^{1}H NMR (DMSO-d_6): δ (ppm) 10.55 (s, 1H), 8.04 (s, 1H), 8.02 (s, 1H), 7.67 (d, 2H, J=8.4Hz), 7.11 (br, 2H), 6.95 (d, 1H, J=8.8Hz), 5.80 (d, 1H, J=6.4Hz), 5.47 (d, 1H, J=5.2Hz), 5.28 (s, 1H), 5.17 (s, 1H), 4.68 (s, 1H), 4.20 (s, 1H), 3.97-3.94 (m, 3H), 3.73-3.61 (m, 2H), 1.76-1.71 (m, 2H), 0.98 (t, 3H, J=7.6Hz); ^{13}C NMR (DMSO-d_6): δ (ppm) 159.13, 156.20, 156.00, 151.02, 140.08, 137.77, 128.03, 127.89, 115.11, 114.54, 87.62, 86.01, 73.16, 71.03, 68.99, 61.92, 22.07, 10.44; HRMS (ESI+) m/z $[M + H]^+$ calculated for $C_{20}H_{25}N_7O_5$: 444.1990; found: 444.1990.

(2R,3R,4S,5R)-2-(6-amino-2-(2-((E)-3-ethoxy-4-hydroxybenzylidene)hydrazineyl)-9H-purin-9-yl)-5-(hydroxymethyl)tetrahydrofuran-3,4-diol (**19**). 43% yield as a white solid; m.p. 198℃; ^{1}H NMR (DMSO-d_6): δ (ppm) 10.43 (s, 1H), 9.19 (s, 1H), 7.99 (s, 1H), 7.94 (s, 1H), 7.66 (s, 1H),

7.04 (br, 2H), 6.92 (d, 1H, J=8.0Hz), 6.77 (d, 1H, J=8.4Hz), 5.75 (d, 1H, J=7.2Hz), 5.48 (d, 1H, J=6.4Hz), 5.44-5.43 (m, 1H), 5.14 (d, 1H, J=4.0Hz), 4.86-4.84 (m, 1H), 4.17 (s, 1H), 4.09 (q, 2H, J=6.8Hz), 4.00 (s, 1H), 3.72-3.52 (m, 2H), 1.37 (t, 3H, J=6.8Hz); ^{13}C NMR (DMSO-d_6): δ (ppm) 156.45, 156.22, 150.75, 147.74, 147.17, 140.93, 138.41, 127.11, 121.14, 115.57, 115.13, 109.94, 88.38, 86.37, 72.43, 71.33, 63.64, 62.46, 14.88; HRMS (ESI+) m/z $[M + H]^+$ calculated for $C_{19}H_{23}N_7O_6$: 446.1783; found: 446.1782.

(2R,3R,4S,5R)-2-(6-amino-2-(2-((E)-3-(benzyloxy)benzylidene)hydrazineyl)-9H-purin-9-yl)-5-(hydroxymethyl)tetrahydrofuran-3,4-diol (**20**). 43% yield as a white solid; m.p. 148℃; ^{1}H NMR (DMSO-d_6): δ (ppm) 10.73 (s, 1H), 8.05 (s, 2H), 7.62-6.95 (m, 11H), 5.79 (d, 1H, J=6.8Hz), 5.48 (d, 1H, J=6.0Hz), 5.38 (s, 1H), 5.16 (s, 3H), 4.79-4.75 (m, 1H), 4.19 (s, 1H), 3.98 (s, 1H), 3.74-3.55 (m, 2H); ^{13}C NMR (DMSO-d_6): δ (ppm) 158.68, 156.17, 150.83, 139.96, 138.30, 137.14, 137.06, 129.66, 128.52, 127.91, 127.81, 119.88, 115.76, 115.55, 111.22, 87.99, 86.14, 72.87, 71.18, 69.21, 62.23; HRMS (ESI+) m/z $[M + H]^+$ calculated for $C_{24}H_{25}N_7O_5$: 492.1990; found: 492.1990.

(2R,3R,4S,5R)-2-(6-amino-2-(2-((E)-4-((4-fluorobenzyl)oxy)benzylidene)hydrazineyl)-9H-purin-9-yl)-5-(hydroxymethyl)tetrahydrofuran-3,4-diol (**21**). 34% yield as a white solid; m.p. 144℃; ^{1}H NMR (DMSO-d_6): δ (ppm) 10.51 (s, 1H), 8.02 (s, 2H), 7.68 (d, 2H, J=8.8Hz), 7.54-7.50 (m, 2H), 7.26-7.22 (m, 2H), 7.04 (d, 4H, J=8.8Hz), 5.80 (d, 1H, J=6.8Hz), 5.47 (d, 1H, J=6.4Hz), 5.31-5.28 (m, 1H), 5.16 (d, 1H, J=4.0Hz), 5.12 (s, 2H), 4.70-4.66 (m, 1H), 4.22-4.19 (m, 1H), 3.98-3.96 (m, 1H), 3.74-3.57 (m, 2H); ^{13}C NMR (DMSO-d_6): δ (ppm) 163.13, 160.61, 158.65, 156.45, 156.22, 151.02, 139.79, 137.75, 133.23, 130.12, 130.04, 128.55, 127.85, 115.42, 115.21, 114.91, 87.67, 86.05, 73.14, 71.08, 68.56, 61.98; HRMS (ESI+) m/z $[M + H]^+$ calculated for $C_{24}H_{24}FN_7O_5$: 510.1896; found: 510.1895.

(2R,3R,4S,5R)-2-(6-amino-2-(2-((E)-4-(benzyloxy)-3-methoxybenzylidene)hydrazineyl)-9H-purin-9-yl)-5-(hydroxymethyl)tetrahydrofuran-3,4-diol (**22**). 32% yield as a white solid; m.p. 146℃; ^{1}H NMR (DMSO-d_6): δ (ppm) 10.54 (s, 1H), 8.00 (s, 1H), 7.99 (s, 1H), 7.77 (s, 1H), 7.47-4.33 (m, 5H), 7.06 (br, 2H), 7.03 (s, 2H), 5.75 (d, 1H, J=7.2H), 5.48 (d, 1H, J=6.4Hz), 5.46 (d, 1H, J=4.0Hz), 5.13 (d, 1H, J=4.0Hz), 5.11 (s, 2H), 4.90-4.85 (m, 1H), 4.17-4.15 (m, 1H), 3.99 (s,

1H), 3.85 (s, 3H), 3.74-3.53 (m, 2H); ^{13}C NMR (DMSO-d_6): δ (ppm) 156.36, 156.22, 150.69, 149.40, 148.46, 140.42, 138.47, 137.00, 128.82, 128.42, 127.87, 120.70, 115.64, 112.92, 108.57, 88.41, 86.34, 72.38, 71.31, 69.86, 62.44, 55.41; HRMS (ESI+) m/z $[M + H]^+$ calculated for $C_{25}H_{27}N_7O_6$: 522.2096; found: 522.2096.

(2R,3R,4S,5R)-2-(6-amino-2-(2-((E)-3,4-bis(benzyloxy)benzylidene)hydrazineyl)-9H-purin-9-yl)-5-(hydroxymethyl)tetrahydrofuran-3,4-diol (**23**). 55% yield as a white solid; m.p. 220℃; ^{1}H NMR (DMSO-d_6): δ (ppm) 10.55 (s, 1H), 8.00 (s, 1H), 7.98 (s, 1H), 7.96 (s, 1H), 7.52-7.30 (m, 10H), 7.09-7.05 (m, 4H), 5.76 (d, 1H, J=7.2Hz), 5.49-5.47 (m, 2H), 5.19-5.14 (m, 5H), 4.89-4.84 (m, 1H), 4.20-4.18 (m, 1H), 4.00 (s, 1H), 3.76-3.54 (m, 2H); ^{13}C NMR (DMSO-d_6): δ (ppm) 156.36, 156.24, 150.71, 148.82, 148.58, 140.30, 138.66, 137.29, 137.23, 128.95, 128.50, 128.44, 127.89, 127.83, 127.72, 127.52, 121.10, 115.68, 113.79, 110.67. 88.39, 86.34, 72.51, 71.37, 69.94, 62.52; HRMS (ESI+) m/z $[M + H]^+$ calculated for $C_{31}H_{31}N_7O_6$: 598.2409; found: 598.2408. HPLC purity：98.08%.

(2R,3R,4S,5R)-2-(6-amino-2-(2-((E)-4-(diethylamino)benzylidene)hydrazineyl)-9H-purin-9-yl)-5-(hydroxymethyl)tetrahydrofuran-3,4-diol (**24**). 39% yield as a white solid; m.p. 164℃; ^{1}H NMR (DMSO-d_6): δ (ppm) 10.27 (s, 1H), 7.99 (s, 1H), 7.92 (s, 1H), 7.51 (d, 2H, J=8.8Hz), 6.99 (br, 2H), 6.66 (d, 2H, J=8.8Hz), 5.78 (d, 1H, J=6.8Hz), 5.47 (d, 1H, J=6Hz), 5.30-5.26 (m, 1H), 5.15 (d, 1H, J=4.4Hz), 4.69-4.65 (m, 1H), 4.21-4.18 (m, 1H), 3.97-3.95 (m, 1H), 3.73-3.56 (m, 2H), 3.39-3.34 (m, 4H), 1.10 (t, 6H, J=6.8Hz); ^{13}C NMR (DMSO-d_6): δ (ppm) 156.59, 156.17, 151.11, 147.76, 141.12, 137.46, 128.00, 122.30, 115.00, 111.13, 87.59, 86.05, 73.16, 71.08, 61.98, 43.72, 12.56; HRMS (ESI+) m/z $[M + H]^+$ calculated for $C_{21}H_{28}N_8O_4$: 457.2306; found: 457.2305. HPLC purity：98.67%.

(2R,3R,4S,5R)-2-(6-amino-2-(2-((E)-4-(pyrrolidin-1-yl)benzylidene)hydrazineyl)-9H-purin-9-yl)-5-(hydroxymethyl)tetrahydrofuran-3,4-diol (25). 46% yield as a white solid; m.p. 174℃; ^{1}H NMR (DMSO-d_6): δ (ppm) 10.23 (s, 1H), 7.98 (s, 1H), 7.94 (s, 1H), 7.54 (d, 2H, J=8.8Hz), 6.95 (br, 2H), 6.54 (d, 2H, J=8.8Hz), 5.78 (d, 1H, J=6.8Hz), 5.44 (d, 1H, J=6.4Hz), 5.27-5.24 (m, 1H), 5.11 (d, 1H, J=4.0Hz), 4.69-4.65 (m, 1H), 4.20 (s, 1H), 3.97 (s, 1H), 3.73-3.57 (m, 2H),

3.26 (s, 4H), 1.96 (s, 4H); ^{13}C NMR (DMSO-d_6): δ (ppm) 156.59, 156.15, 151.08, 147.91, 141.29, 137.42, 127.77, 122.55, 115.00, 111.51, 87.65, 86.03, 73.16, 71.04, 61.96, 47.24, 24.97; HRMS (ESI+) m/z $[M + H]^+$ calculated for $C_{21}H_{26}N_8O_4$: 455.2150; found: 455.2150.

(2R,3R,4S,5R)-2-(6-amino-2-(2-((E)-4-morpholinobenzylidene)hydrazineyl)-9H-purin-9-yl)-5-(hydroxymethyl)tetrahydrofuran-3,4-diol (**26**). 44% yield as a white solid; m.p. 186℃; ^{1}H NMR (DMSO-d_6): δ (ppm) 10.42 (s, 1H), 8.01 (s, 1H), 7.97 (s, 1H), 7.59 (d, 2H, J=8.4Hz), 7.02 (br, 2H), 6.95 (d, 2H, J=8.8Hz), 5.79 (d, 1H, J=6.4Hz), 5.46 (d, 1H, J=6.0Hz), 5.29-5.26 (m, 1H), 5.15 (d, 1H, J=4.0Hz), 4.69-4.65 (m, 1H), 4.21-4.18 (m, 1H), 3.97-3.95 (m, 1H), 3.74 (t, 4H, J=8.4Hz), 3.71-3.56 (m, 2H), 3.17 (t, 4H, J=8.8Hz); ^{13}C NMR (DMSO-d_6): δ (ppm) 156.47, 156.19, 151.11, 151.04, 140.34, 137.57, 127.43, 126.29, 115.13, 114.56, 87.63, 86.01, 73.14, 71.04, 66.03, 61.95, 47.85; HRMS (ESI+) m/z $[M + H]^+$ calculated for $C_{21}H_{26}N_8O_5$: 471.2099; found: 471.2100.

N-(4-((E)-(2-(6-amino-9-((2R,3R,4S,5R)-3,4-dihydroxy-5-(hydroxymethyl)tetrahydrofuran-2-yl)-9H-purin-2-yl)hydrazono)methyl)phenyl)acetamide (**27**). 23% yield as a white solid; m.p. 126℃; ^{1}H NMR (DMSO-d_6): δ (ppm) 10.54 (s, 1H), 10.03 (s, 1H), 8.02 (s, 2H), 7.66-7.59 (m, 4H), 7.03 (br, 2H), 5.79 (d, 1H, J=6.4Hz), 5.44 (d, 1H, J=6.0Hz), 5.24-5.21 (m, 1H), 5.11 (d, 1H, J=4.4), 4.67 (dd, 1H, J=5.6Hz,5.6Hz), 4.24-4.21 (m, 1H), 3.98-3.96 (m, 1H), 3.75-3.57 (m, 2H), 2.06 (s, 3H); ^{13}C NMR (DMSO-d_6): δ (ppm) 168.31, 156.45, 156.15, 150.94, 139.75, 139.54, 137.76, 130.31, 126.88, 118.85, 115.15, 87.75, 85.95, 73.12, 71.00, 61.93, 24.06; HRMS (ESI+) m/z $[M + H]^+$ calculated for $C_{19}H_{22}N_8O_5$: 443.1786; found: 443.1786.

(2R,3R,4S,5R)-2-(6-amino-2-(2-((E)-4-(pyridin-2-yl)benzylidene)hydrazineyl)-9H-purin-9-yl)-5-(hydroxymethyl)tetrahydrofuran-3,4-diol (**28**). 69% yield as a white solid; m.p. 164℃; ^{1}H NMR (DMSO-d_6): δ (ppm) 10.83 (s, 1H), 8.69 (s, 1H), 8.15-7.85 (m, 8H), 7.36-7.35 (m, 1H), 7.18 (br, 2H), 5.83 (d, 1H, J=6.4Hz), 5.50 (s, 1H), 5.28 (s, 1H), 5.20 (s, 1H), 4.71 (s, 1H), 4.25 (s, 1H), 4.00 (s, 1H), 3.77-3.62 (m, 2H); ^{13}C NMR (DMSO-d_6): δ (ppm) 156.15, 155.51, 150.98, 149.63, 139.38, 138.36, 138.01, 137.30, 136.27, 126.74, 122.69. 120.23, 115.39, 97.71, 86.02,

73.19, 71.05, 61.96; HRMS (ESI+) m/z $[M + H]^+$ calculated for $C_{22}H_{22}N_8O_4$: 463.1837; found: 463.1838.

(2R,3R,4S,5R)-2-(2-(2-((E)-4-(1H-imidazol-1-yl)benzylidene)hydrazineyl)-6-amino-9H-purin-9-yl)-5-(hydroxymethyl)tetrahydrofuran-3,4-diol (**29**). 81% yield as a white solid; m.p. 276℃; ^{1}H NMR (DMSO-d_6): δ (ppm) 10.77 (s, 1H), 8.33 (s, 1H), 8.11 (s, 1H), 8.05 (s, 1H), 7.89 (d, 2H, J=8.4Hz), 7.81 (s, 1H), 7.70 (d, 2H, J=8.8Hz), 7.13 (s, 1H), 7.11 (br, 2H), 5.81 (d, 1H, J=6.8Hz), 5.48 (d, 1H, J=6.4Hz), 5.35-5.32 (m, 1H), 5.19 (d, 1H, J=4.0Hz), 4.74-4.70 (m, 1H), 4.22-4.20 (m, 1H), 3.99 (s, 1H), 3.76-3.59 (m, 1H); ^{13}C NMR (DMSO-d_6): δ (ppm) 156.26, 150.90, 138.72, 138.03, 136.56, 135.50, 134.18, 130.00, 127.70, 120.28, 117.86, 115,49, 87.77, 86.13, 73.06, 71.12, 62.04; HRMS (ESI+) m/z $[M + H]^+$ calculated for $C_{20}H_{21}N_9O_4$: 452.1789; found: 452.1789.

(2R,3R,4S,5R)-2-(2-(2-((E)-[1,1'-biphenyl]-4-ylmethylene)hydrazineyl)-6-amino-9H-purin-9-yl)-5-(hydroxymethyl)tetrahydrofuran-3,4-diol (**30**). 60% yield as a white solid; m.p. 234℃; ^{1}H NMR (DMSO-d_6): δ (ppm) 10.78 (s, 1H), 8.12 (s, 1H),8.07 (s, 1H), 7.83 (d, 2H, J=8.4Hz), 7.31-7.71 (m, 4H), 7.48 (t, 2H, J=7.2Hz), 7.38 (t, J=7.2Hz,1H), 7.16 (br, 2H), 5.82 (d, 1H, J=6.8Hz), 5.49 (d, 1H, J=6.0Hz), 5.28 (s, 1H), 5.19 (d, 1H, J=4.4Hz), 4.69-4.67 (m, 1H), 4.22 (d, 1H, J=2.4Hz), 3.98 (d, 1H, J=2.4Hz), 3.75-3.60 (m, 2H); ^{13}C NMR (DMSO-d_6): δ (ppm) 156.09, 151.00, 139.94, 139.63, 139.50, 137.92, 134.75, 129.03, 127.64, 126.99, 126.86, 126.57, 115.30, 97.59, 86.01, 73.20, 71.04, 61.95; HRMS (ESI+) m/z $[M + H]^+$ calculated for $C_{23}H_{23}N_7O_4$: 462.1884; found: 462.1884. HPLC purity：96.08%.

(2R,3R,4S,5R)-2-(6-amino-2-(2-((E)-4-(diphenylamino)benzylidene)hydrazineyl)-9H-purin-9-yl)-5-(hydroxymethyl)tetrahydrofuran-3,4-diol (**31**). 42% yield as a yellow solid; m.p. 184℃; ^{1}H NMR (DMSO-d_6): δ (ppm) 10.56 (s, 1H), 8.01 (s, 2H), 7.63 (d, 2H,J=8.4Hz), 7.35-6.94 (m, 14H), 5.77 (d, 1H,J=6.4Hz), 5.45 (d, 1H,J=6.0Hz), 5.27-5.24 (m, 1H), 5.11 (d, 1H,J=4.4Hz), 4.70-4.66 (m, 1H), 4.21-4.18 (m, 1H), 3.93 (d, 1H,J=2.4Hz), 3.73-3.53 (m, 2H); ^{13}C NMR (DMSO-d_6): δ (ppm) 156.24, 148.37, 147.55, 146.86, 146.71, 140.36, 138.83, 129.68, 128.57, 127.91, 127.64, 124.63, 124.40, 123.73, 123.46, 122.40, 121.99, 114.31, 87.92, 85.65, 73.09,

71.00, 61.93; HRMS (ESI+) m/z $[M + H]^+$ calculated for $C_{29}H_{28}N_8O_4$: 553.2306; found: 553.2306. HPLC purity：95.71%.

(2R,3R,4S,5R)-2-(2-(2-((E)-(1H-pyrrol-2-yl)methylene)hydrazineyl)-6-amino-9H-purin-9-yl)-5-(hydroxymethyl)tetrahydrofuran-3,4-diol (**32**). 30% yield as a white solid; m.p. 220℃; ^{1}H NMR (DMSO-d_6): δ (ppm) 11.69 (s, 1H), 10.55 (s, 1H), 7.94 (s, 1H), 7.87 (s, 1H), 7.07 (br, 2H), 6.94 (s, 1H), 6.61-6.59 (m, 1H), 6.26 (s, 1H), 6.07 (dd, 1H, J=3.2Hz,2.8Hz), 5.71 (d, 1H, J=8.0Hz), 5.39 (d, 1H, J=6.8Hz), 5.21 (d, 1H, J=3.6Hz), 4.88 (dd, 1H, J=4.8Hz,7.2Hz), 4.18 (dd, 1H, J=4Hz), 4.09 (s, 1H), 3.82-3.74 (m, 2H); ^{13}C NMR (DMSO-d_6): δ (ppm) 151.61, 150.37, 148.90, 139.90, 136.45, 127.33, 122.41, 113.59, 112.21, 109.31, 87.04, 85.48, 74.07, 70.13, 61.07; HRMS (ESI+) m/z $[M + H]^+$ calculated for $C_{15}H_{18}N_8O_4$: 375.1524; found: 375.1524.

(2R,3R,4S,5R)-2-(6-amino-2-(2-((E)-thiazol-5-ylmethylene)hydrazineyl)-9H-purin-9-yl)-5-(hydroxymethyl)tetrahydrofuran-3,4-diol (**33**). 56% yield as a white solid; m.p. 88℃; ^{1}H NMR (DMSO-d_6): δ (ppm) 10.97 (s, 1H), 9.04 (s, 1H), 8.36 (s, 1H), 8.09 (s, 2H), 7.24 (br, 2H), 5.80 (d, 1H, J=6.4Hz), 5.47 (s, 1H), 5.16 (s, 2H), 4.61 (s, 1H), 4.19 (s, 1H), 3.95 (d, 1H, J=3.2Hz), 3.72-3.57 (m, 2H); ^{13}C NMR (DMSO-d_6): δ (ppm) 155.90, 155.56, 154.41, 151.02, 143,16, 137.88, 136.03, 132.50, 115.13, 87.31, 85.80, 73.37, 70.83, 61.83; HRMS (ESI+) m/z $[M + H]^+$ calculated for $C_{14}H_{16}N_8O_4S$: 393.1088; found: 393.1089.

(2R,3R,4S,5R)-2-(6-amino-2-(2-((E)-(2-butyl-5-chloro-1H-imidazol-4-yl)methylene)-hydrazineyl) -9H-purin-9-yl)-5-(hydroxymethyl)tetrahydrofuran-3,4-diol (**34**). 58% yield as a white solid; m.p. 188℃; ^{1}H NMR (DMSO-d_6): δ (ppm) 12.70 (s, 1H), 10.85 (s, 1H), 7.99 (s, 1H), 7.88 (s, 1H), 7.18 (br, 2H), 6.75 (d, 1H, J=10.0Hz), 5.73 (d, 1H, J=8.0Hz), 5.42 (d, 1H, J=6.4Hz), 5.24 (s, 1H), 4.90-4.85 (m, 1H), 4.17 (s, 1H), 4.11 (s, 1H), 3.86-3.72 (m, 2H), 2.64 (t, 2H, J=7.6Hz), 1.63 (quint, 2H, J=7.6Hz), 1.33 (sext, 2H, J=7.6Hz); ^{13}C NMR (DMSO-d_6): δ (ppm) 156.40, 156.15, 150.06, 148.73, 139.29, 127.066, 126.90, 122.87, 116.20, 89.08, 86.41, 71.88, 71.59, 62.82, 29.76, 27.93, 21.63, 12,72; HRMS (ESI+) m/z $[M + H]^+$ calculated for $C_{18}H_{24}ClN_9O_4$: 466.1713; found: 466.1714.

(2R,3R,4S,5R)-2-(6-amino-2-(2-((E)-(5-(4-bromophenyl)furan-2-yl)methylene)hydrazineyl)-9H-purin-9-yl)-5-(hydroxymethyl)tetrahydrofuran-3,4-diol (**35**). 17% yield as a yellow solid;

m.p. 200℃; ^{1}H NMR (DMSO-d_6): δ (ppm) 10.77 (s, 1H), 8.05 (s, 1H), 8.02 (s, 1H), 7.76 (d, 2H, J=8.8Hz), 7.64 (d, 2H, J=8.8Hz), 7.13 (d, 1H, J=3.6Hz), 7.09 (br, 2H), 6.91 (d, 1H, J=3.6Hz), 5.81 (d, 1H, J=6.4Hz), 5.46 (d, 1H, J=6Hz), 5.14-5.08 (m, 2H), 4.72-4.67 (m, 1H), 4.25-4.22 (m, 1H), 3.98-3.97 (m, 1H), 3.74-3.58 (m, 2H); ^{13}C NMR (DMSO-d_6): δ (ppm) 156.20, 156.03, 152.07, 150.90, 137.90, 131.85, 129.60, 129.09, 125.58, 120.56, 115.38, 112.14, 10.03, 87.63, 85.90. 73.01, 70.91, 61.95; HRMS (ESI+) m/z $[M + H]^+$ calculated for $C_{21}H_{20}BrN_7O_5$: 530.0782; found: 530.0782.

(2R,3R,4S,5R)-2-(6-amino-2-(2-((E)-(2-chloropyridin-3-yl)methylene)hydrazineyl)-9H-purin-9-yl)-5-(hydroxymethyl)tetrahydrofuran-3,4-diol (**36**). 86% yield as a white solid; m.p. 180℃; ^{1}H NMR (DMSO-d_6): δ (ppm) 11.18 (s, 1H), 8.63 (d, 1H, J=6.4Hz), 8.39 (s, 1H), 8.35 (dd, 1H, J=2.0Hz,2.8Hz), 8.08 (s, 1H), 7.47 (dd, 1H, J=2.8Hz,4.4Hz), 7.19 (br, 2H), 5.80 (d, 1H, J=7.2Hz), 5.46 (d, 1H, J=6.4Hz), 5.37-5.34 (m, 1H), 5.18 (d, 1H, J=4.0Hz), 4.75-4.70 (m, 1H), 4.23-4.20 (m, 1H), 3.99 (s, 1H), 3.75-3.57 (m, 2H); ^{13}C NMR (DMSO-d_6): δ (ppm) 156.32, 155.86, 150.67, 149.05, 148.20, 138.51, 135.34, 134.07, 129.83, 123.56, 115.72, 88.03, 86.13, 72.97, 71.14, 62.02; HRMS (ESI+) m/z $[M + H]^+$ calculated for $C_{16}H_{17}ClN_8O_4$: 421.1134; found: 421.1132.

(2R,3R,4S,5R)-2-(6-amino-2-(2-((E)-(5-bromopyridin-2-yl)methylene)hydrazineyl)-9H-purin-9-yl)-5-(hydroxymethyl)tetrahydrofuran-3,4-diol (**37**). 75% yield as a yellow solid; m.p. 256℃; ^{1}H NMR (DMSO-d_6): δ (ppm) 11.13 (s, 1H), 8.72 (s, 1H), 8.13 (s, 1H), 8.10 (s, 1H), 8.07 (d, 1H, J=1.6Hz), 8.05 (d, 1H, J=2.0Hz), 7.40 (br, 2H), 5.81 (d, 1H, J=6.4Hz), 5.47 (d, 1H, J=4.4Hz), 5.32 (s, 1H), 5.19 (s, 1H), 4.70 (s, 1H), 4.21 (s, 1H), 3.98 (s, 1H), 3.74-3.60 (m, 2H); ^{13}C NMR (DMSO-d_6): δ (ppm) 156.21, 155.68, 153.30, 150.76, 149.89, 139.15, 139.06, 138.35, 121.36, 119.03, 115.66, 87.72, 86.,03, 73.09, 71.03, 61.92; HRMS (ESI+) m/z $[M + H]^+$ calculated for $C_{16}H_{17}BrN_8O_4$: 465.0629; found: 465.0628.

(2R,3R,4S,5R)-2-(6-amino-2-(2-((E)-(6-methoxypyridin-3-yl)methylene)hydrazineyl)-9H-purin-9-yl)-5-(hydroxymethyl)tetrahydrofuran-3,4-diol (**38**). 63% yield as a white solid; m.p. 226℃; ^{1}H NMR (DMSO-d_6): δ (ppm) 8.43 (s, 2H), 8.19 (s, 1H), 8.10 (s, 1H), 6.88 (d, 1H,

J=8.4Hz), 5.79 (d, 1H, J=6Hz), 5.51 (s, 1H), 5.22 (s, 2H), 4.62 (s, 1H), 4.19 (d, 1H), 3.98-3.96 (m, 1H), 3.89 (s, 3H), 3.72-3.57 (m, 2H); ^{13}C NMR (DMSO-d_6): δ (ppm) 163.95, 150.94, 146.71, 138.78, 136.45, 124.87, 111.03, 87.56, 85.92, 73.41, 70.78, 61.66, 53.48; HRMS (ESI+) m/z $[M + H]^+$ calculated for $C_{17}H_{20}N_8O_5$: 417.1629; found: 417.1631.

(2R,3R,4S,5R)-2-(6-amino-2-(2-((E)-quinolin-6-ylmethylene)hydrazineyl)-9H-purin-9-yl)-5-(hydroxymethyl)tetrahydrofuran-3,4-diol (**39**). 52% yield as a white solid; m.p. 260℃; ^{1}H NMR (DMSO-d_6): δ (ppm) 10.87 (s, 1H), 8.87 (dd, 1H, J=2.4Hz,2.0Hz), 8.38-8.35 (m, 2H), 8.28 (s, 1H), 8.11 (d, 1H, J=1.6Hz), 8.06 (s, 1H), 8.01 (d, 1H, J=8.8Hz), 7.54 (dd, 1H, J=4.4Hz,4.0Hz), 7.11 (br, 2H), 5.84 (d, 1H, J=6.4Hz), 5.47 (d, 1H, J=6.4Hz), 5.30 (dd, 1H, J=2.8Hz,4.8Hz), 5.16 (d, 1H, 4.4Hz), 4.73 (dd, 1H, J=4.8Hz,6.4Hz), 4.28 (dd, 1H, J=2.4Hz,4.8Hz), 4.02-4.00 (m, 1H), 3.81-3.63 (m, 2H); ^{13}C NMR (DMSO-d_6): δ (ppm) 156.28, 156.20, 150.90, 150.43, 147.91, 138.99, 138.07, 136.05, 133.95, 129.20, 128.10, 126.80, 126.38, 121.90, 115.55, 87.90, 86.03, 73.12, 71.06, 62.00; HRMS (ESI+) m/z $[M + H]^+$ calculated for $C_{20}H_{20}N_8O_4$: 437.1680; found: 437.1682.

(2R,3R,4S,5R)-2-(6-amino-2-(2-((E)-3-(methylthio)propylidene)hydrazineyl)-9H-purin-9-yl)-5-(hydroxymethyl)tetrahydrofuran-3,4-diol (**40**). 18% yield as a white solid; m.p. 138℃; ^{1}H NMR (DMSO-d_6): δ (ppm) 10.21 (s, 1H), 7.99 (s, 1H), 7.34 (t, 1H, J=5.6Hz), 6.99 (s, 2H), 5.75 (d, 1H, J=6.8Hz), 5.40 (d, 1H, J=6Hz), 5.14-5.11 (m, 2H), 4.59 (dd, 1H, J=6.4Hz,5.2Hz), 4.12 (dd, 1H, J=4.4Hz,2.4Hz), 3.93-3.90 (m, 1H), 3.67-3.50 (m, 2H), 2.64 (t, 2H, J=8Hz), 2.51-2.47 (m, 2H), 2.08 (s, 3H); ^{13}C NMR (DMSO-d_6): δ (ppm) 156.64, 156.24, 151.21, 141.64, 137.25, 114.82, 87.06, 85.88, 73.14, 70.87, 61.89, 31.66, 30.88, 14.64; HRMS (ESI+) m/z $[M + H]^+$ calculated for $C_{14}H_{21}N_7O_4S$: 384.1448; found: 384.1448.

(2R,3R,4S,5R)-2-(6-amino-2-(2-((E)-cyclopentylmethylene)hydrazineyl)-9H-purin-9-yl)-5-(hydroxymethyl)tetrahydrofuran-3,4-diol (**41**). 27% yield as a white solid; m.p. 170℃; ^{1}H NMR (DMSO-d_6): δ (ppm) 10.02 (s, 1H), 7.99 (s, 1H), 7.24 (d, 1H J=6.8Hz), 6.97 (br, 2H), 5.76 (d, 1H, J=6.4Hz), 5.42 (d, 1H, J=6.8Hz), 5.14-5.08 (m, 2H), 4.56 (dd, 1H, J=4.8Hz,6.8Hz), 4.14-4.11 (m, 1H), 3.92-3.89 (m, 1H), 3.66-3.51 (m, 2H), 2.71-2.61 (m, 1H), 1.83-1.39 (m, 8H);

^{13}C NMR (DMSO-d_6): δ (ppm) 156.68, 156.20, 151.30, 147.11, 137.00, 114.56, 86.87, 85.76, 73.18, 70.57, 61.66, 42.29, 30.75, 24.97; HRMS (ESI+) m/z $[M + H]^+$ calculated for $C_{16}H_{23}N_7O_4$: 378.1884; found: 378.1887.

(2R,3R,4S,5R)-2-(6-amino-2-(2-((E)-3-(4-isopropylphenyl)-2-methylpropylidene)-hydrazineyl)-9H-purin-9-yl)-5-(hydroxymethyl)tetrahydrofuran-3,4-diol (**42**). 19% yield as a white solid; m.p. 142℃; ^{1}H NMR (DMSO-d_6): δ (ppm) 10.11 (s, 1H), 8.00 (s, 1H), 7.31-7.12 (m, 5H), 7.00 (br, 2H), 5.77-5.76 (m, 1H), 5.41 (d, 1H, J=5.6Hz), 5.13 (d, 2H, J=4.4Hz), 4.61-4.58 (m, 1H), 4.14 (s, 1H), 3.92 (s, 1H), 3.67-3.53 (m, 2H), 2.87-2.54 (m, 4H), 1.17 (d, 6H, J=7.2Hz), 1.00 (d, 3H, J=6.4Hz); ^{13}C NMR (DMSO-d_6): δ (ppm) 156.53, 156.08, 151.22, 147.45, 145.84, 137.26, 137.17, 129.11, 126.13, 114.75, 114.68, 87.05, 85.77, 73.18, 70.87, 61.86, 40.23, 37.80, 33.05, 24.00, 18.15; HRMS (ESI+) m/z $[M + H]^+$ calculated for $C_{23}H_{31}N_7O_4$: 470.2510; found: 470.2510. HPLC purity：96.94%.

(2R,3R,4S,5R)-2-(6-amino-2-(2-((1E,2E,4E)-deca-2,4-dien-1-ylidene)hydrazineyl)-9H-purin-9-yl)-5-(hydroxymethyl)tetrahydrofuran-3,4-diol (**43**). 23% yield as a brown solid; m.p. 166℃; ^{1}H NMR (DMSO-d_6): δ (ppm) 10.50 (s, 1H), 8.04 (s, 1H), 7.71 (d, 1H, J=8.8Hz), 7.06 (br, 2H), 6.44-6.18 (m, 3H), 5.89-5.81 (m, 1H), 5.77 (d, 1H, J=6.8Hz), 5.41 (d, 1H, J=6.4Hz), 5.16 (d, 1H, J=4.0Hz), 5.11-5.08 (m, 1H), 4.60-4.56 (m, 1H), 4.12 (s, 1H), 3.92 (s, 1H), 3.67-3.52 (m, 2H), 2.13-2.08 (m, 2H), 1.98-1.28 (m, 6H), 0.87 (t, 3H, J=7.2Hz); ^{13}C NMR (DMSO-d_6): δ (ppm) 156.22, 151.25, 141.92, 137.29, 136.77, 135.30, 130.39, 128.10, 114.96, 86.79, 85.76, 73.22, 70.77, 61.81, 32.31, 30.96, 28.42, 22.03, 14.01; HRMS (ESI+) m/z $[M + H]^+$ calculated for $C_{20}H_{29}N_7O_4$: 432.2354; found: 432.2355.

4.3 Biological activity.

4.3.1 Materials.

[3H] DPCPX (cyclopentyl-1,3-dipropylxanthine, 8-[dipropyl-2,3-3H(N)]-; specific activity, 250 μCi) and [3H] CGS 21680 (2-[p-(2-carboxyethyl)phenethylamino]-5'-N-ethylcarboxamidoadenosine, [Carboxyethyl-3H(N)]-; specific activity, 250 μCi) were obtained from PerkinElmer Research

Products (Boston, MA). The cell membranes were prepared from HEK-293 cells stably-transfected with A_{2A} (human) adenosine receptor and adenosine A_1 (human) membranes were prepared from CHO-K1 cells. Cell membranes were obtained from PerkinElmer Research Products (Boston, MA). DPCPX(cyclopentyl-1,3-dipropylxanthine) and CGS 21680 (2-[p-(2-carboxyethyl)phenethylamino]-5'-nethylcarboxamidoadenosine) were obtained from Sigma (St. Louis, MO, USA) and Selleck (Shanghai, CN), respectively. All other reagents were of analytical grade and were obtained from commercial sources.

4.3.2 Human Cloned A_1AR and A_{2A}AR Binding Assay.

All synthesized compounds were tested to evaluate their affinity for the A_1AR and A_{2A}AR expressed on cell membranes. Three-fold serial dilution of the compounds in a 384-well Opti-Plate using Echo550 was performed to generate a compound source plate with 10 different concentrations. The membranes were diluted in 1mL of assay buffer (50 mM Tris-HCl pH 7.4, 10 mM $MgCl_2$, 1 mM EDTA, 1 μg/mL Adenosine Deaminase) with [3H] DPCPX (5 nM) for the hA_1 CHO membranes and [3H] CGS 21680 (25 nM) for the hA_{2A} HEK-293 membranes. The diluted membranes were transferred to a 384-well solid Opti-Plate containing novel compounds and incubated at 27℃ for 60 min. Bound radioactivity and free radioactivity were separated by filtering the assay mixture through a UNIFILTER-96 GF/B filter plate and washing with wash buffer (50 mM Tris-HCl pH 7.4, 154 mM NaCl). ULTIMA GOLD was added to the filter plate of membranes, and the count per minute (CPM) was read using MicroBeta.

4.3.3 Measurement of Cyclic AMP Levels in HEK 293 Cells.

Cells stably expressing human A_{2A} adenosine receptor were cultured in complete medium at 37℃ under 5% CO_2, detached using Versene Solution, collected by centrifugation at 200g at R.T. for 5min and resuspended with assay buffer (Hank's buffered saline solution, 1M HEPES, 7.5% BSA stabilizer pH 7.4, 20mM rolipram). Three-fold serial dilution of the compounds with DMSO in a 384-well polypropylene microplate was performed using the TECAN EVO system to generate a compound source plate with 11 concentrations. A test compound from the compound source plate was dispensed onto the assay plate to serve as the subsequent plate layout by Echo, at 10 nl/well. The hA_{2A} HEK-293 cells (300 cells/well) were suspended in assay buffer (Hank's buffered saline solution, 1M HEPES, 20mM Rolipram, 7.5% BSA stabilizer pH 7.4),

centrifuged at 150g for 1 min, and preincubated at room temperature for 30 min. The potency expressed as the EC_{50} (nM) of the novel compounds versus A_{2A}ARs was determined by stimulation of cyclic AMP levels. Eu-cAMP tracer working solution (5 μl/well) was added to the assay plate, and the Ulight-anti-cAMP working solution (5 μl/well) was added to the assay plate. The assay plate was centrifuged at 150g for 30 sec and incubated at R.T. for 30 min. The final aqueous solution was tested for cyclic AMP levels using EnVison (λ_{ex}=320 nm, λ_{em}= 665 nm and 615 nm).

4.3.4 Data Analysis.

Inhibitory binding constant (K_i) values were calculated from those of the IC_{50} according to the Cheng and Prusoff equation $K_i = IC_{50}/(1+[S]/K_M)$ [31], where [S] is the concentration of the radioligand and K_M is a dissociation constant of 2.28 nM (human A_1AR) for [3H] DPCPX[32] and 22 nM (human A_{2A}AR) for [3H]CGS21680[33, 34]. The statistical software package GraphPad Prism 6.0 was used for computer-based analysis of the binding experiments. Functional experiments were analyzed by using the statistical software XLfit. All experimental data are expressed as the mean ± standard error of the mean (SEM).

Acknowledgments

We are grateful for the financial supports of the National Science and Technology Major Projects for "Major New Drugs Innovation and Development" (2018ZX09711003) of China.

References

[1] B.B. Fredholm, I.J. AP, K.A. Jacobson, J. Linden, C.E. Muller, International Union of Basic and Clinical Pharmacology. LXXXI. Nomenclature and classification of adenosine receptors--an update, Pharmacol. Rev., 63 (2011) 1-34.
[2] B.B. Fredholm, Adenosine receptors as drug targets, Exp. Cell Res., 316 (2010) 1284-1288.
[3] M. de Lera Ruiz, Y.H. Lim, J. Zheng, Adenosine A2A receptor as a drug discovery target, J. Med. Chem., 57 (2014) 3623-3650.
[4] J.F. Chen, H.K. Eltzschig, B.B. Fredholm, Adenosine receptors as drug targets--what are the challenges?, Nat. Rev. Drug Discov., 12 (2013) 265-286.
[5] C.E. Muller, K.A. Jacobson, Recent developments in adenosine receptor ligands and their potential as novel drugs, Biochim. Biophys. Acta, 1808 (2011) 1290-1308.
[6] G. Yuan, G.B. Jones, Towards next generation adenosine A(2A) receptor antagonists, Curr. Med. Chem., 21 (2014) 3918-3935.

[7] M.D. Valls, B.N. Cronstein, M.C. Montesinos, Adenosine receptor agonists for promotion of dermal wound healing, Biochem. Pharmacol., 77 (2009) 1117-1124.
[8] K. Varani, G. Caramori, F. Vincenzi, A. Tosi, A. Barczyk, M. Contoli, P. Casolari, M. Triggiani, T. Hansel, E. Leung, S. Maclennan, P.J. Barnes, K.F. Chung, I. Adcock, A. Papi, P.A. Borea, Oxidative/nitrosative stress selectively altered A(2B) adenosine receptors in chronic obstructive pulmonary disease, FASEB J., 24 (2010) 1192-1204.
[9] G. Hasko, J. Linden, B. Cronstein, P. Pacher, Adenosine receptors: therapeutic aspects for inflammatory and immune diseases, Nat. Rev. Drug Discov., 7 (2008) 759-770.
[10] R. Akkari, J.C. Burbiel, J. Hockemeyer, C.E. Muller, Recent progress in the development of adenosine receptor ligands as antiinflammatory drugs, Curr. Top. Med. Chem., 6 (2006) 1375-1399.
[11] M.P. Bosch, F. Campos, I. Niubo, G. Rosell, J.L. Diaz, J. Brea, M.I. Loza, A. Guerrero, Synthesis and biological activity of new potential agonists for the human adenosine A2A receptor, J. Med. Chem., 47 (2004) 4041-4053.
[12] M. Rivera-Oliver, M. Diaz-Rios, Using caffeine and other adenosine receptor antagonists and agonists as therapeutic tools against neurodegenerative diseases: a review, Life Sci., 101 (2014) 1-9.
[13] M. Congreve, S.P. Andrews, A.S. Dore, K. Hollenstein, E. Hurrell, C.J. Langmead, J.S. Mason, I.W. Ng, B. Tehan, A. Zhukov, M. Weir, F.H. Marshall, Discovery of 1,2,4-triazine derivatives as adenosine A(2A) antagonists using structure based drug design, J. Med. Chem., 55 (2012) 1898-1903.
[14] A.S. Dore, N. Robertson, J.C. Errey, I. Ng, K. Hollenstein, B. Tehan, E. Hurrell, K. Bennett, M. Congreve, F. Magnani, C.G. Tate, M. Weir, F.H. Marshall, Structure of the adenosine A(2A) receptor in complex with ZM241385 and the xanthines XAC and caffeine, Structure, 19 (2011) 1283-1293.
[15] T. Hino, T. Arakawa, H. Iwanari, T. Yurugi-Kobayashi, C. Ikeda-Suno, Y. Nakada-Nakura, O. Kusano-Arai, S. Weyand, T. Shimamura, N. Nomura, A.D. Cameron, T. Kobayashi, T. Hamakubo, S. Iwata, T. Murata, G-protein-coupled receptor inactivation by an allosteric inverse-agonist antibody, Nature, 482 (2012) 237-240.
[16] V.P. Jaakola, M.T. Griffith, M.A. Hanson, V. Cherezov, E.Y. Chien, J.R. Lane, A.P. Ijzerman, R.C. Stevens, The 2.6 angstrom crystal structure of a human A2A adenosine receptor bound to an antagonist, Science, 322 (2008) 1211-1217.
[17] G. Lebon, P.C. Edwards, A.G. Leslie, C.G. Tate, Molecular Determinants of CGS21680 Binding to the Human Adenosine A2A Receptor, Mol. Pharmacol., 87 (2015) 907-915.
[18] G. Lebon, T. Warne, P.C. Edwards, K. Bennett, C.J. Langmead, A.G. Leslie, C.G. Tate, Agonist-bound adenosine A2A receptor structures reveal common features of GPCR activation, Nature, 474 (2011) 521-525.
[19] W. Liu, E. Chun, A.A. Thompson, P. Chubukov, F. Xu, V. Katritch, G.W. Han, C.B. Roth, L.H. Heitman, I.J. AP, V. Cherezov, R.C. Stevens, Structural basis for allosteric regulation of GPCRs by sodium ions, Science, 337 (2012) 232-236.
[20] E. Segala, D. Guo, R.K. Cheng, A. Bortolato, F. Deflorian, A.S. Dore, J.C. Errey, L.H. Heitman, I.J. AP, F.H. Marshall, R.M. Cooke, Controlling the Dissociation of Ligands from the Adenosine A2A Receptor through Modulation of Salt Bridge Strength, J. Med. Chem., 59 (2016) 6470-6479.
[21] F. Xu, H. Wu, V. Katritch, G.W. Han, K.A. Jacobson, Z.G. Gao, V. Cherezov, R.C. Stevens, Structure of an agonist-bound human A2A adenosine receptor, Science, 332 (2011) 322-327.

[22] A.J. Hutchison, R.L. Webb, H.H. Oei, G.R. Ghai, M.B. Zimmerman, M. Williams, CGS 21680C, an A2 selective adenosine receptor agonist with preferential hypotensive activity, J. Pharmacol. Exp. Ther, 251 (1989) 47-55.
[23] M.F. Jarvis, R. Schulz, A.J. Hutchison, U.H. Do, M.A. Sills, M. Williams, [3H]CGS 21680, a selective A2 adenosine receptor agonist directly labels A2 receptors in rat brain, J. Pharmacol. Exp. Ther, 251 (1989) 888-893.
[24] X. Liu, A.L. Gentzler, P. Tepper, E. Kiss, V.O. Kothencne, Z. Tamas, A. Vetro, M. Kovacs, Clinical features of depressed children and adolescents with various forms of suicidality, J. Clin. Psychiatry, 67 (2006) 1442-1450.
[25] V.P. Palle, E.O. Elzein, S.A. Gothe, Z. Li, Z. Gao, S. Meyer, B. Blackburn, J.A. Zablocki, Structure-affinity relationships of the affinity of 2-pyrazolyl adenosine analogues for the adenosine A2A receptor, Bioorg. Med. Chem. Lett., 12 (2002) 2935-2939.
[26] J. Zablocki, V. Palle, B. Blackburn, E. Elzein, G. Nudelman, S. Gothe, Z. Gao, Z. Li, S. Meyer, L. Belardinelli, 2-substituted pi system derivatives of adenosine that are coronary vasodilators acting via the A2A adenosine receptor, Nucleos. Nucleot. Nucl, 20 (2001) 343-360.
[27] D.G. Kim, M.S. Bynoe, A2A adenosine receptor modulates drug efflux transporter P-glycoprotein at the blood-brain barrier, J. Clin. Invest., 126 (2016) 1717-1733.
[28] X.Q. Lewell, D.B. Judd, S.P. Watson, M.M. Hann, RECAP--retrosynthetic combinatorial analysis procedure: a powerful new technique for identifying privileged molecular fragments with useful applications in combinatorial chemistry, J. Chem. Inf. Comput. Sci., 38 (1998) 511-522.
[29] M. Zhang, C.Q. Sheng, H. Xu, Y.L. Song, W.N. Zhang, Constructing virtual combinatorial fragment libraries based upon MDL Drug Data Report database, Sci. China Ser. B-Chem., 50 (2007) 364-371.
[30] W.J. Allen, T.E. Balius, S. Mukherjee, S.R. Brozell, D.T. Moustakas, P.T. Lang, D.A. Case, I.D. Kuntz, R.C. Rizzo, DOCK 6: Impact of new features and current docking performance, J. Comput. Chem., 36 (2015) 1132-1156.
[31] B.T. Burlingham, T.S. Widlanski, An intuitive look at the relationship of Ki and IC50: a more general use for the Dixon plot, J. Chem. Edu., 80 (2003) 214-218.
[32] F. Libert, J. Van Sande, A. Lefort, A. Czernilofsky, J.E. Dumont, G. Vassart, H.A. Ensinger, K.D. Mendla, Cloning and functional characterization of a human A1 adenosine receptor, Biochem. Biophys. Res. Commun., 187 (1992) 919-926.
[33] K. Varani, P.A. Borea, L. Guerra, S. Dionisotti, C. Zocchi, E. Ongini, Binding characteristics of the adenosine A2 receptor ligand [3H]CGS 21680 to human platelet membranes, Biochem. Pharmacol., 48 (1994) 1658-1661.
[34] W. Wan, G.R. Sutherland, J.D. Geiger, Binding of the adenosine A2 receptor ligand [3H]CGS 21680 to huamn and rat brain: evidence for multiple affinity sites, J. Neurochem., 55 (1990) 1763-1771.
[35] Z. Gao, Z. Li, S.P. Baker, R.D. Lasley, S. Meyer, E. Elzein, V. Palle, J.A. Zablocki, B. Blackburn, L. Belardinelli, Novel short-acting A2A adenosine receptor agonists for coronary vasodilation: inverse relationship between affinity and duration of action of A2A agonists, J. Pharmacol. Exp. Ther, 298 (2001) 209-218.

Figure 1. The structures of specific potent and selective A_{2A}AR agonists.

Figure 2. Molecular derivative design strategy using CombLig and the design flow chart.

Scheme 1. Synthesis of Target Compounds **12-43** [a]. **[a]** Reagents and conditions: (a) SnCl4, RT->90℃；90℃；90℃->120℃；120℃，15min；MeOH, cooled；(b) NH3，MeOH，100 ℃，24h; 100℃->RT; RT，24h；(c) N2H4.H2O，EtOH，50℃, 4h；(d) MeOH，80℃ microwave，30min.

Table 1. The binding affinity (K_i) of the test compounds for hA_1 and hA_{2A} adenosine receptors.

Table 2. Binding affinities and Functional Potencies of Compounds **21, 23, 30, 32, 34, 41, 42**, and **43.**

Figure 3. The binding mode of the cocrystallized ligand UK432097 (**5)** (a) and the predicted binding modes of the four compounds discovered in the FBSD (b). The A_{2A}AR binding site is shown in multicolor ribbons with the side chains of THR88, LEU167, PHE168, GLU169, LEU249, ASN253, TYR271, ILE274, SER277 and HIS278 in sticks. In (a), the cocrystallized ligand **5** is shown using black carbon atoms, and docking compound **3** is shown using green carbon atoms. Dotted lines indicate interactions. In (b), the docking orientations for compounds **12, 21, 23** and **30** are shown with blue, green, red and purple lines, respectively. In (c), the docking compound **23** is shown using green carbon atoms. In (d), interactions of docking compound 23 with the A_{2A}AR are depicted in a 2D diagram.

Figure 4. Statistical analysis of the interacting residues. In (a)-(d), residue-interaction histograms show nonbond receptor-ligand interactions for compounds **12-43** according to the results of docking. The following interaction types are included in the histograms: favorable (a), charge (b), hydrogen bond (c), and hydrophobic (d). In (e), a heat map shows the significant residues of the A_{2A}AR involved in favorable nonbond interactions with docking compounds **12-43**.

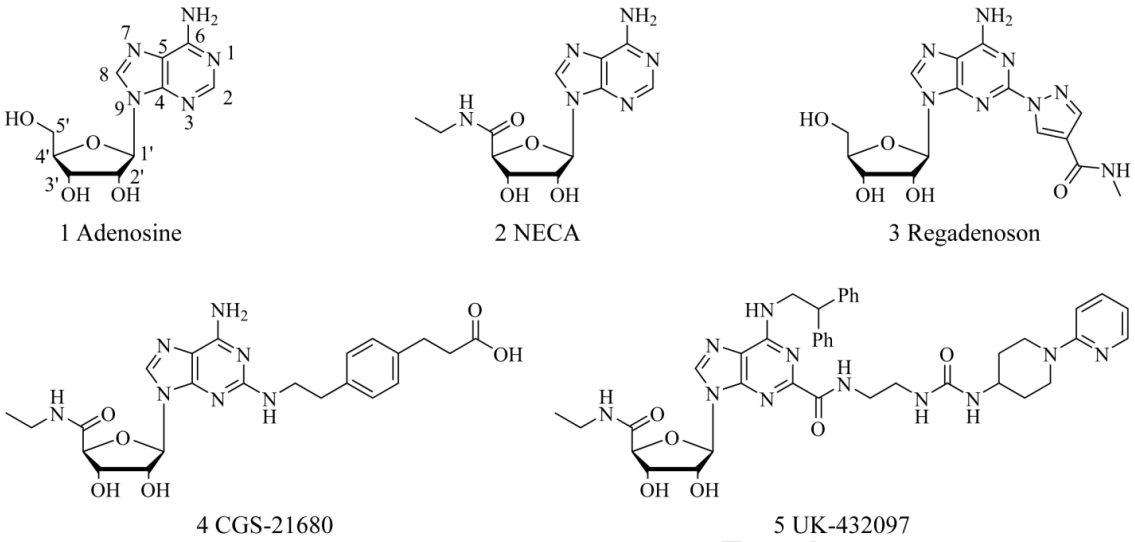

Figure 1. The structures of specific potent and selective $A_{2A}AR$ agonists.

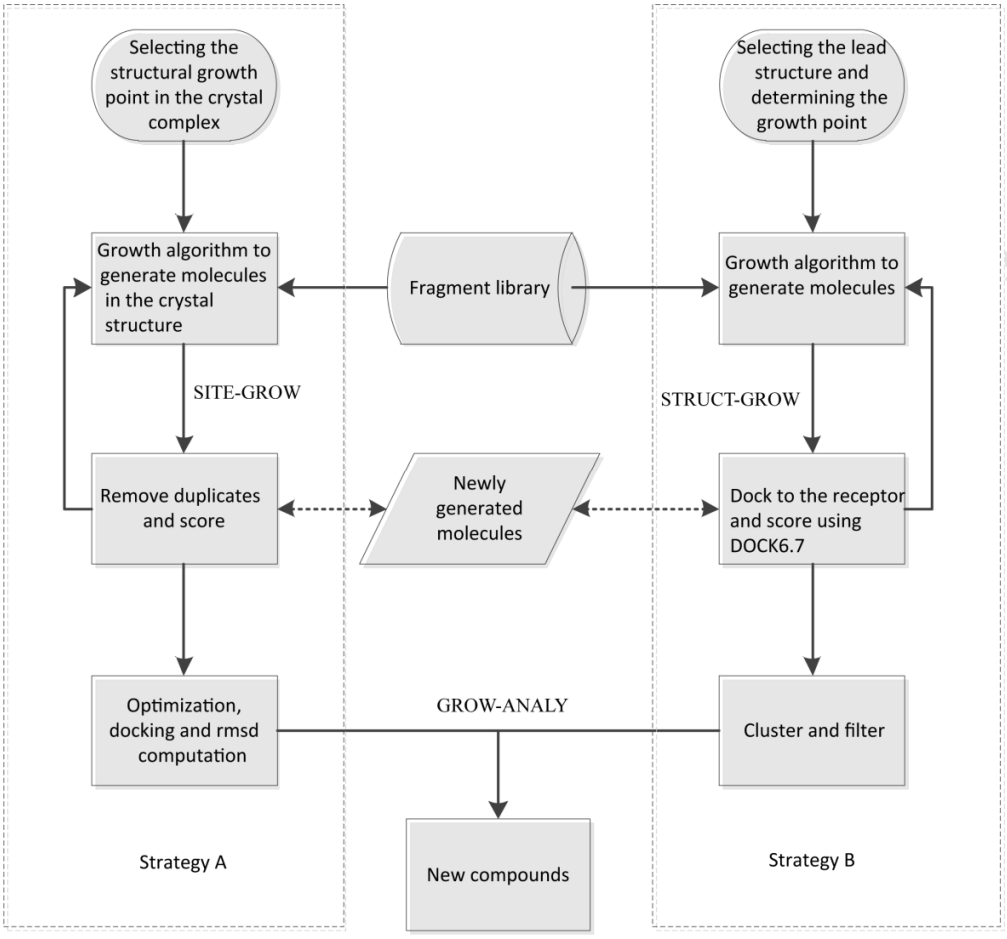

Figure 2. Molecular derivative design strategy using CombLig and the design flow chart.

Scheme 1. Synthesis of Target Compounds **12-43** [a]

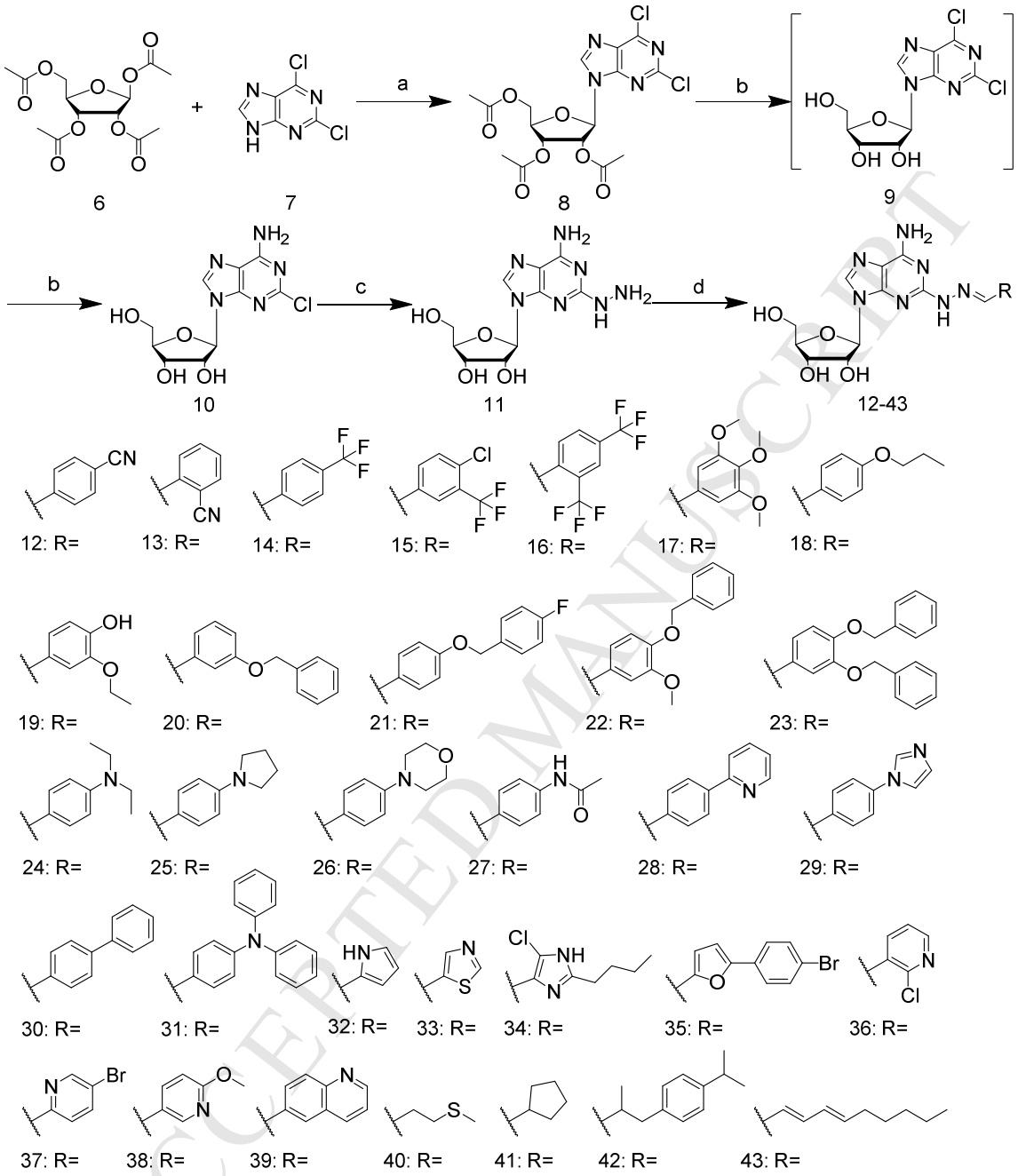

[a] Reagents and conditions: (a) SnCl4, RT->90℃; 90℃; 90℃->120℃; 120℃, 15min; MeOH, cooled; (b) NH3, MeOH, 100℃, 24h; 100℃->RT; RT, 24h; (c) N2H4.H2O, EtOH, 50℃, 4h; (d) MeOH, 80℃ microwave, 30min.

Table 1. The binding affinity (K_i) of the test compounds for hA_1 and hA_{2A} adenosine receptors.

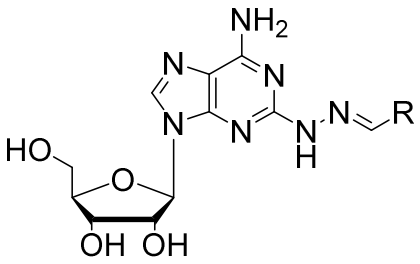

Compound	R	K_i±SEM (nM) or (% disp. at 1 μM)[a]		SI[d] (A_1/A_{2A})
		hA_1[b]	hA_{2A}[c]	
1	—	310[e]	700[e]	0.44
3	—	> 16460[f]	1269[f]	> 13
4	—	290[e]	27[e]	10.7
12	4-cyano-phenyl	4.1 ± 3.1	8.5 ± 0.4	0.5
13	2-cyano-phenyl	2.9 ± 0.3	1306 ± 2	0.002
14	4-(trifluoromethyl)phenyl	37 ± 3	61 ± 2	0.6
15	4-chloro-3-(trifluoromethyl)phenyl	> 10000 (11%)	801 ± 1	> 1000
16	2,4-bis(trifluoromethyl)phenyl	> 10000 (0%)	6276 ± 2	> 1000
17	3,4,5-trimethoxyphenyl	> 10000 (0%)	5495 ± 3	> 1000
18	4-propoxyphenyl	> 10000 (7%)	224 ± 0.1	66
19	3-ethoxy-4-hydroxyphenyl	6944 ± 2	1622 ± 1	5
20	3-(benzyloxy)phenyl	13 ± 3	173 ± 1	0.075
21	4-((4-fluorobenzyl)oxy)phenyl	70 ± 6	5.5 ± 2.0	12.5
22	4-(benzyloxy)-3-methoxyphenyl	9142 ± 2	101 ± 2	91
23	3,4-bis(benzyloxy)phenyl	> 10000 (0%)	1.8 ± 1.3	> 1000
24	4-(diethylamino)phenyl	> 10000 (0%)	6.4 ± 2	> 1000
25	4-(pyrrolidin-1-yl)phenyl	5.1 ± 3.8	6625 ± 3	0.00077
26	4-morpholinophenyl	2.5 ± 2	800 ± 2	0.003

27	4-(acetamido)phenyl	> 10000 (0%)	1329 ± 1	> 1000
28	4-(pyridin-2-yl)phenyl	7536 ± 3	208 ± 1	36
29	4-(1H-imidazol-1-yl) phenyl	> 10000 (0%)	216 ± 1	> 1000
30	[1,1'-biphenyl]-4-yl	7856 ± 2	20 ± 2	0.0025
31	4-(diphenylamino)phenyl	> 10000 (0%)	67 ± 1	> 1000
32	1H-pyrrol-2-yl	8.0 ± 2.2	8.3 ± 1.6	0.96
33	thiazol-5-yl	22 ± 5	71 ± 2	0.31
34	2-butyl-5-chloro-1H-imidazol-4-yl	12 ± 2	18 ± 1	0.67
35	5-(4-bromophenyl)furan-2-yl	4.5 ± 1.8	> 10000 (27%)	< 0.001
36	2-chloropyridin-3-yl	4.6 ± 2.1	8.7 ± 1.9	0.53
37	5-bromopyridin-2-yl	4.7 ± 2	239 ± 1	0.02
38	6-methoxypyridin-3-yl	2.6 ± 1.6	1449 ± 2	0.0018
39	quinolin-6-yl	9.8 ± 1.9	6.5 ± 2.0	1.5
40	2-(methylthio)ethyl	> 10000 (0%)	> 10000 (8%)	—
41	cyclopentyl	5.6 ± 1.8	4.1 ± 1.7	1.4
42	1-(4-isopropylphenyl)-2-propyl	9502 ± 2	6.3 ± 1.4	1429
43	(E)-nona-1,3-dien-1-yl	2.0 ± 8.3	17.5 ± 2	0.11

[a] All values of the binding experiments are expressed as the mean ± SEM of duplicate determinations. The % displacement was determined at the 1 μM concentration of the tested compounds.
[b] Displacement of specific [3H]DPCPX competitive binding to hA_1CHO cells.
[c] Displacement of specific [3H]CGS21680 competitive binding to hA_{2A}HEK-293 cells.
[d] The selectivity index (SI) for the A_{2A} receptor isoform calculated as the ratio K_i (A_1)/K_i (A_{2A}).
[e] Literature values obtained from Ref. [3].
[f] Literature values obtained from Ref. [35].

Table 2. Binding affinities and Functional Potencies of Compounds **21, 23, 30, 32, 34, 41, 42**, and **43.**

Compound	R	binding K_i (nM)	functional EC_{50} (nM)
		hA_{2A}[a]	hA_{2A}[b]
12	4-cyano-phenyl	8.5	15.28
21	4-((4-fluorobenzyl)oxy)phenyl	5.5	4.05
23	3,4-bis(benzyloxy)phenyl	1.8	0.64
24	4-(diethylamino)phenyl	6.4	17.86
30	[1,1'-biphenyl]-4-yl	20	5.70
32	1H-pyrrol-2-yl	8.3	8.52
34	2-butyl-5-chloro-1H-imidazol-4-yl	18	1.10
36	2-chloropyridin-3-yl	8.7	4.60
39	quinolin-6-yl	6.5	5.52
41	cyclopentyl	4.1	4.34
42	1-(4-isopropylphenyl)-2-propyl	6.3	1.38
43	(E)-nona-1,3-dien-1-yl	17.5	10.15

[a] Binding affinities were determined by using membrane preparations from HEK-293 cells overexpressing the hA_{2A}AR.
[b] Cyclic AMP levels were measured by using HEK-293 cells expressing the human A_{2A}AR.

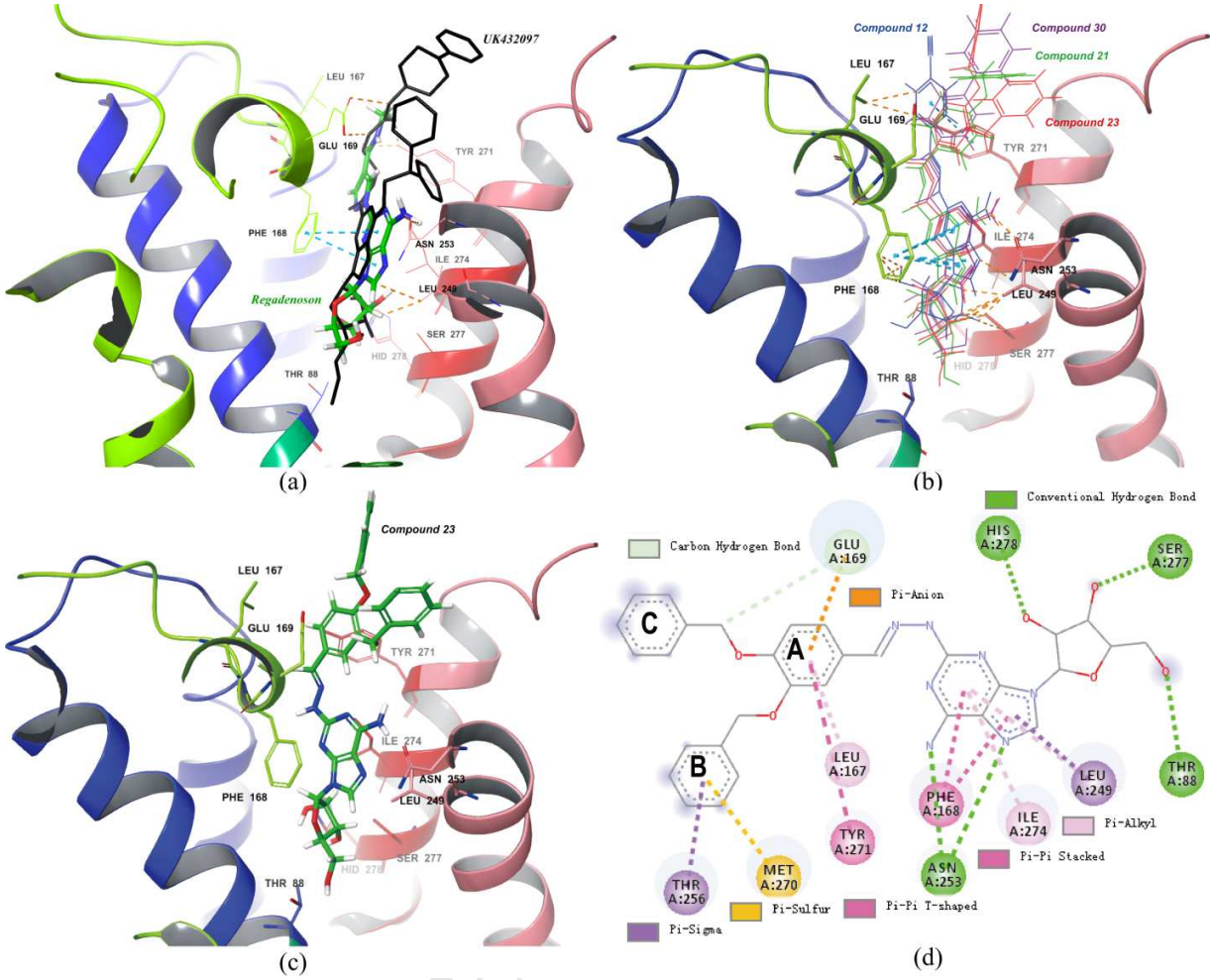

Figure 3. The binding mode of the cocrystallized ligand UK432097 (**5)** (a) and the predicted binding modes of the four compounds discovered in the FBSD (b). The A_{2A}AR binding site is shown in multicolor ribbons with the side chains of THR88, LEU167, PHE168, GLU169, LEU249, ASN253, TYR271, ILE274, SER277 and HIS278 in sticks. In (a), the cocrystallized ligand **5** is shown using black carbon atoms, and docking compound **3** is shown using green carbon atoms. Dotted lines indicate interactions. In (b), the docking orientations for compounds **12, 21, 23** and **30** are shown with blue, green, red and purple lines, respectively. In (c), the docking compound **23** is shown using green carbon atoms. In (d), interactions of docking compound 23 with the A_{2A}AR are depicted in a 2D diagram.

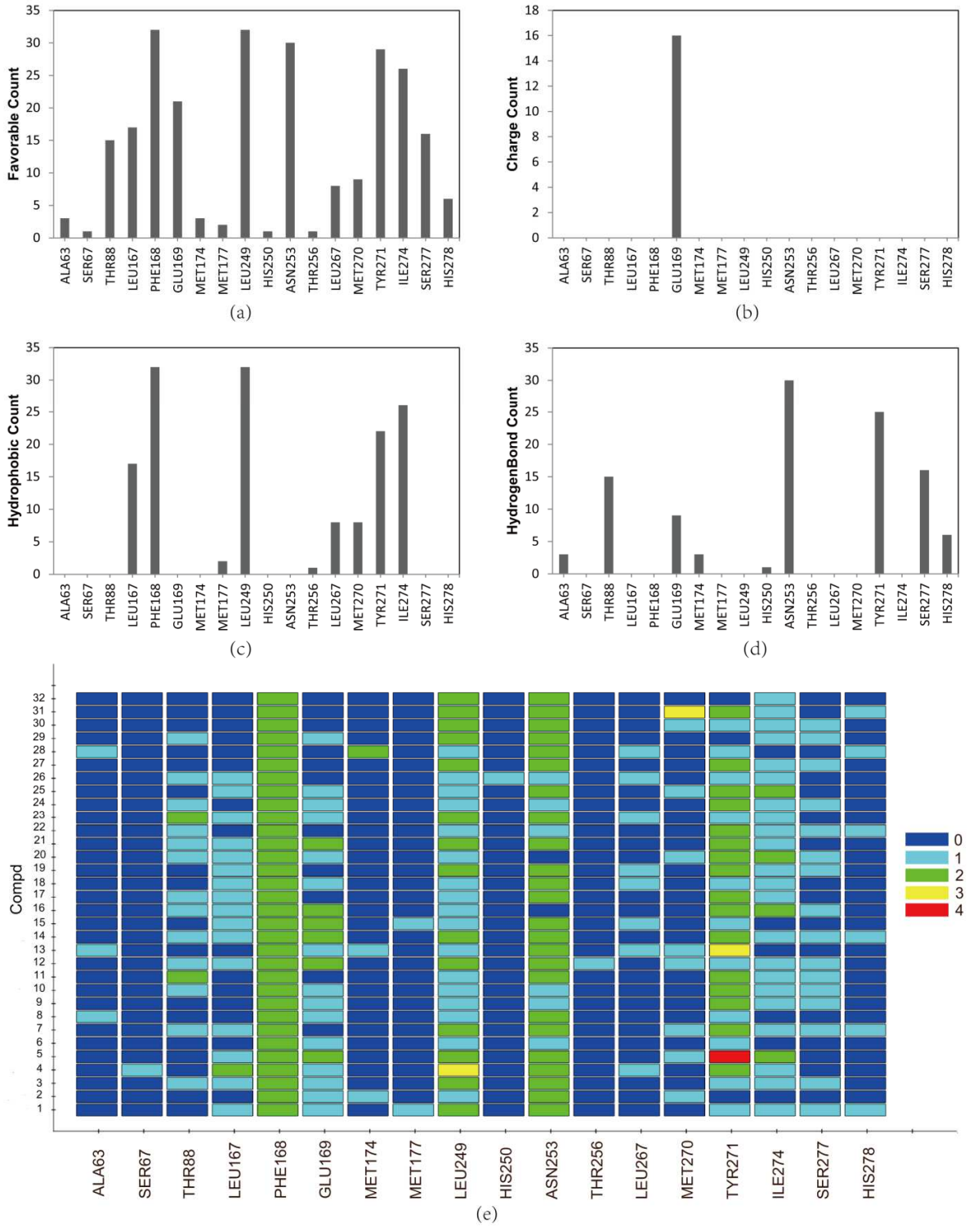

Figure 4. Statistical analysis of the interacting residues. In (a)-(d), residue-interaction histograms show nonbond receptor-ligand interactions for compounds **12-43** according to the results of

docking. The following interaction types are included in the histograms: favorable (a), charge (b), hydrogen bond (c), and hydrophobic (d). In (e), a heat map shows the significant residues of the A_{2A}AR involved in favorable nonbond interactions with docking compounds **12-43**.

Figures and Schemes

Figure 1. The structures of specific potent and selective A_{2A}AR agonists.

Figure 2. Molecular derivative design strategy using CombLig and the design flow chart.

Figure 3. The binding mode of the cocrystallized ligand UK432097 (**5)** (a) and the predicted binding modes of the four compounds discovered in the FBSD (b). The A_{2A}AR binding site is shown in multicolor ribbons with the side chains of THR88, LEU167, PHE168, GLU169, LEU249, ASN253, TYR271, ILE274, SER277 and HIS278 in sticks. In (a), the cocrystallized ligand **5** is shown using black carbon atoms, and docking compound **3** is shown using green carbon atoms. Dotted lines indicate interactions. In (b), the docking orientations for compounds **12, 21, 23** and **30** are shown with blue, green, red and purple lines, respectively. In (c), the docking compound **23** is shown using green carbon atoms. In (d), interactions of docking compound 23 with the A_{2A}AR are depicted in a 2D diagram.

Figure 4. Statistical analysis of the interacting residues. In (a)-(d), residue-interaction histograms show nonbond receptor-ligand interactions for compounds **12-43** according to the results of docking. The following interaction types are included in the histograms: favorable (a), charge (b), hydrogen bond (c), and hydrophobic (d). In (e), a heat map shows the significant residues of the A_{2A}AR involved in favorable nonbond interactions with docking compounds **12-43**.

Scheme 1. Synthesis of Target Compounds **12-43** [a]. [a] Reagents and conditions: (a) SnCl4, RT->90℃；90℃；90℃->120℃；120℃，15min；MeOH, cooled；(b) NH3，MeOH，100 ℃，24h; 100℃->RT; RT，24h；(c) N2H4.H2O，EtOH，50℃，4h；(d) MeOH，80℃ microwave，30min.

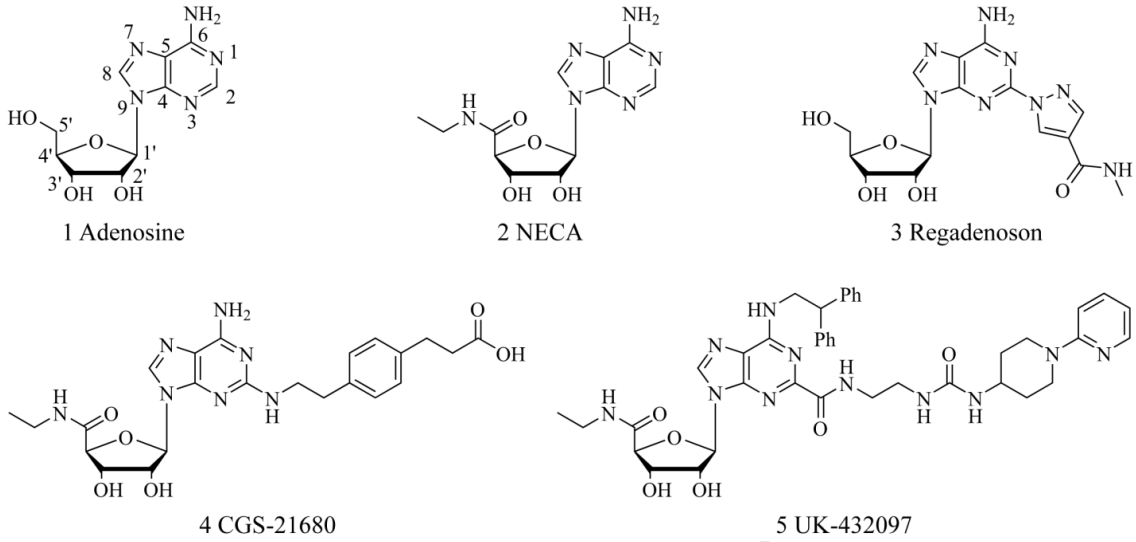

Figure 1. The structures of specific potent and selective A_{2A}AR agonists.

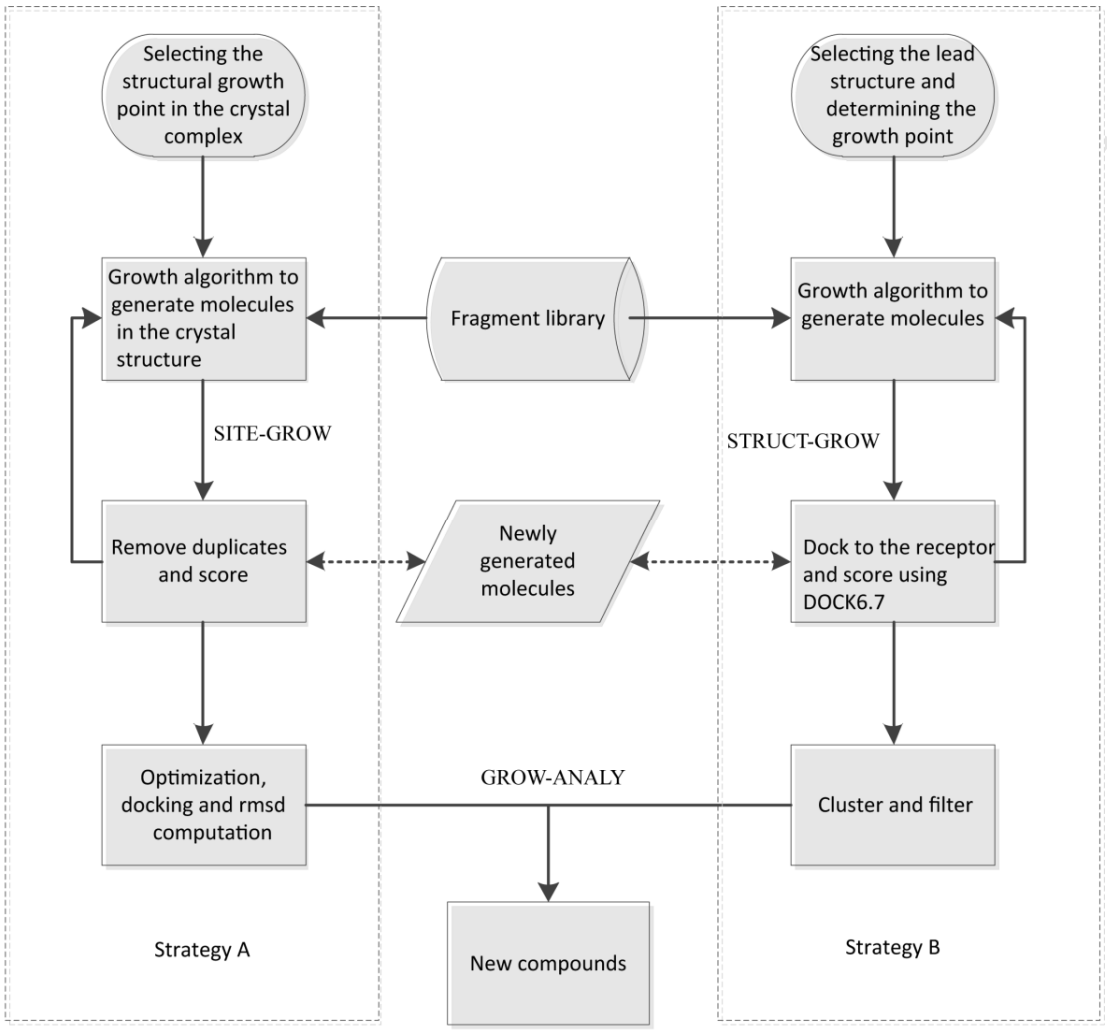

Figure 2. Molecular derivative design strategy using CombLig and the design flow chart.

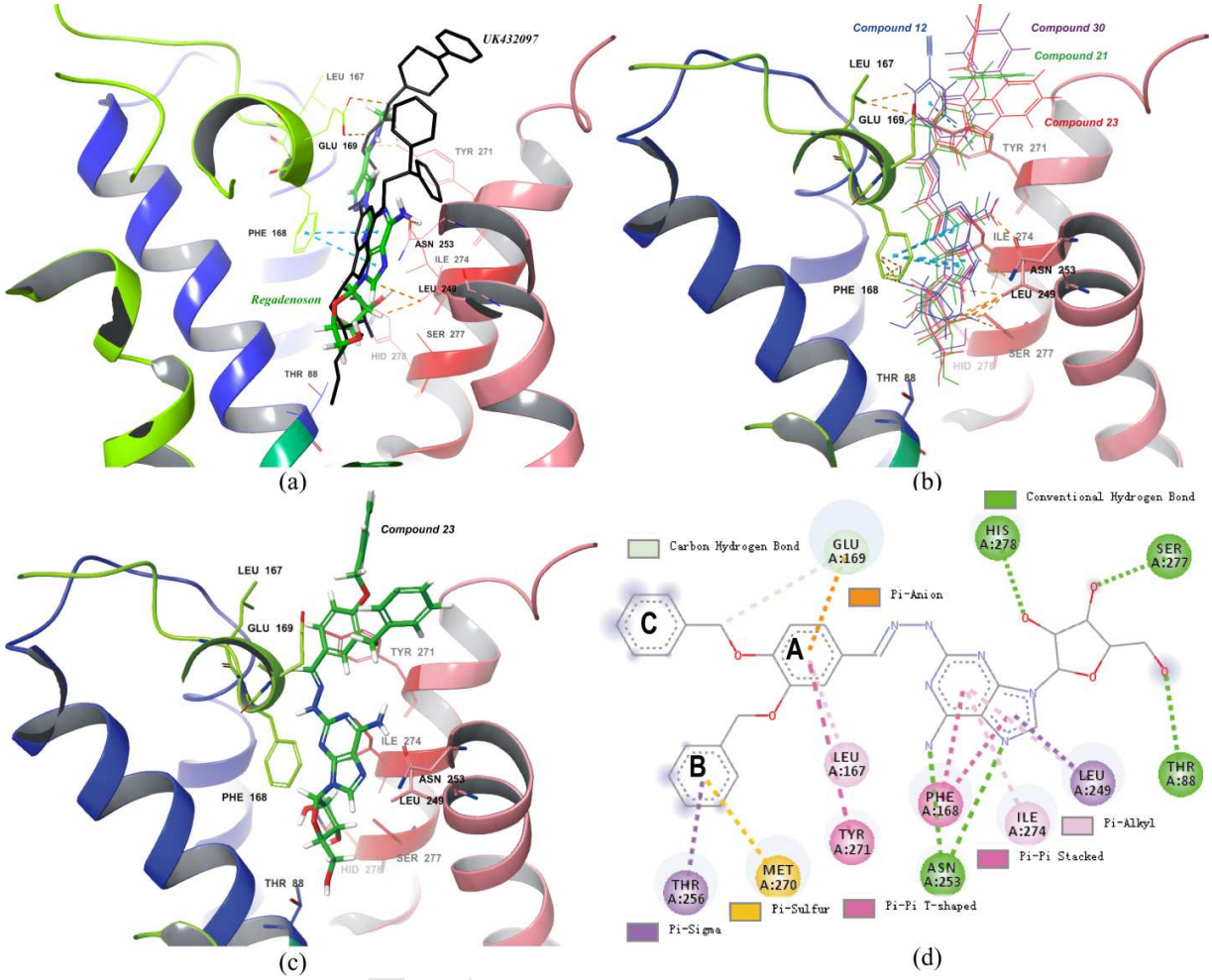

Figure 3. The binding mode of the cocrystallized ligand UK432097 (**5)** (a) and the predicted binding modes of the four compounds discovered in the FBSD (b). The A_{2A}AR binding site is shown in multicolor ribbons with the side chains of THR88, LEU167, PHE168, GLU169, LEU249, ASN253, TYR271, ILE274, SER277 and HIS278 in sticks. In (a), the cocrystallized ligand **5** is shown using black carbon atoms, and docking compound **3** is shown using green carbon atoms. Dotted lines indicate interactions. In (b), the docking orientations for compounds **12, 21, 23** and **30** are shown with blue, green, red and purple lines, respectively. In (c), the docking compound **23** is shown using green carbon atoms. In (d), interactions of docking compound 23 with the A_{2A}AR are depicted in a 2D diagram.

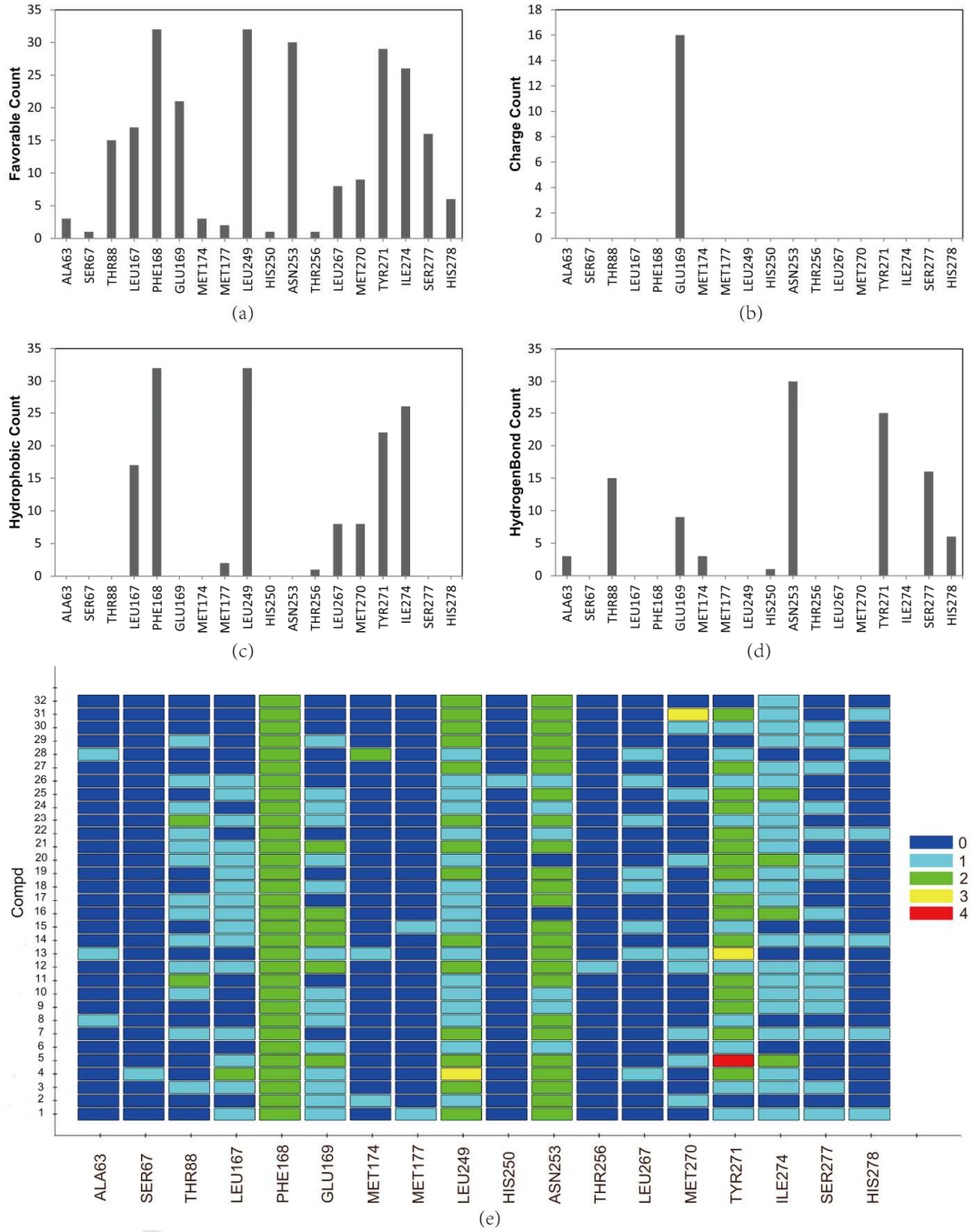

Figure 4. Statistical analysis of the interacting residues. In (a)-(d), residue-interaction histograms show nonbond receptor-ligand interactions for compounds **12-43** according to the results of docking. The following interaction types are included in the histograms: favorable (a), charge (b), hydrogen bond (c), and hydrophobic (d). In (e), a heat map shows the significant residues of the $A_{2A}AR$ involved in favorable nonbond interactions with docking compounds **12-43**.

Scheme 1. Synthesis of Target Compounds **12-43** [a]

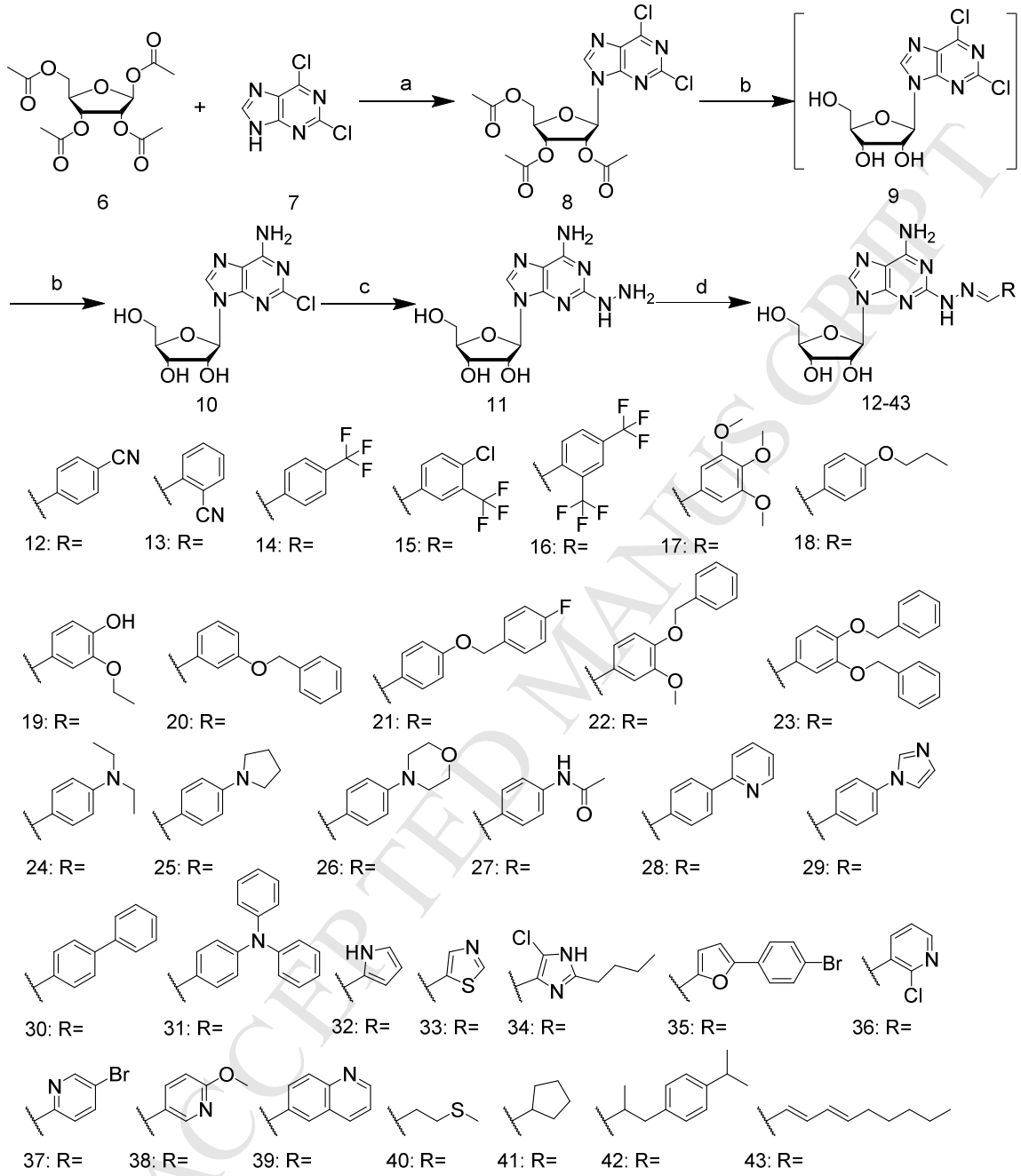

[a] Reagents and conditions: (a) SnCl4, RT->90℃; 90℃; 90℃->120℃; 120℃, 15min; MeOH, cooled; (b) NH3, MeOH, 100℃, 24h; 100℃->RT; RT, 24h; (c) N2H4.H2O, EtOH, 50℃, 4h; (d) MeOH, 80℃ microwave, 30min.

Highlights

- Synthesis of novel potent A_{2A}AR agonists with high affinities.
- Agonists design based on fragment-based drug design and fragment libraries.
- Compound 23 exhibiting a K_i value of 1.8 nM for A_{2A}AR and significant selectivity for the A_{2A} receptor compared to the A_1 receptor(SI> 1000).
- Compound 35 has a high A_1 receptor selectivity, with a K_i value for the A_1 receptor of 4.5 nM.